Exacerbation of blood brain barrier dysfunction and brain injury after aneurysmal subarachnoid hemorrhage in endothelial specific S1PR1 knock out mice.

Akira Ito[1,4], Hiroki Uchida[1], Gab Seok Kim[1, #], Giuseppe Faraco[2], Richard Proia[3], Kuniyasu Niizuma[4], Teiji Tominaga[4], Josef Anrather[2], Costantino Iadecola[2], Michael J Kluk[1] and Teresa Sanchez[1,2,*] .

[1]Department of Pathology and Laboratory Medicine, Center for Vascular Biology, Weill Cornell Medicine, New York, NY

[2]Department of Neuroscience, Brain and Mind Research Institute, Weill Cornell Medicine, New York, NY.

[3]Genetics of Development and Disease Branch, NIDK, NIH, Bethesda, MD.

[4] Tohoku University, Sendai, Japan

#Current address: Department of Neurology, UTHealth, McGovern Medical School, Houston TX.

* Correspondence to: Teresa Sanchez, PhD. Department of Pathology and Laboratory Medicine, Center for Vascular Biology and Department of Neuroscience, Brain and Mind Research Institute, Weill Cornell Medicine, 1300 York Ave, A607B, New York, NY 10065.

ABSTRACT

Blood brain barrier (BBB) dysfunction upon ischemia and hypoxia has been implicated in the exacerbation of neuronal injury in stroke. Despite the therapeutic potential of the cerebrovascular endothelium, the limited understanding of the endothelial signaling pathways governing BBB function restricts progress towards developing novel therapeutic approaches specifically targeting the endothelium in stroke. Sphingosine-1-phosphate (S1P) is a potent modulator of endothelial function via its receptors (S1PR). Recent human and mouse studies indicate that anti-inflammatory endothelial S1P signaling via S1PR1 is limiting in cardiovascular and inflammatory diseases. Herein, we aimed to investigate the expression of S1PR1 in the mouse and human brain and the role of endothelial-specific S1PR1 signaling in BBB function, neuronal injury and neurological outcomes in a mouse model of aneurysmal subarachnoid hemorrhage (SAH), the most devastating type of stroke. We found that S1PR1 is the most abundant S1PR transcript in the mouse brain and in mouse and human brain endothelial cells (20-100 mRNA copies per cell). S1PR1 transcripts were significantly enriched (~6 fold) in mouse cortical microvessels compared to total brain. Using the S1PR1-eGFP knock in mouse, we found that S1PR1-eGFP is abundantly expressed in the cerebrovascular endothelium and neurons in the mouse brain. A similar pattern of expression was observed in human brain autopsy samples. Endothelial specific deletion of S1PR1, induced in adult mice (*S1pr1* $^{flox/flox}$*x Cdh5-Cre*^{ERT2}*,* referred to as *S1pr1*^{iECKO}) by tamoxifen administration, resulted in exacerbation of brain edema, neuronal injury as well as worsened neurological outcomes upon SAH compared to *S1pr1* $^{flox/flox}$ littermates. No differences in the SAH grade, hemostasis in the tail bleeding assay or cerebral blood flow changes during and after SAH were found between groups. Mechanistically, *S1pr1*^{iECKO} exhibited aggravated BBB dysfunction and increased phosphorylation of myosin light chain (MLC) in isolated cortical microvessels, a downstream effector of the Rho-ROCK pathway implicated in endothelial inflammation and barrier dysfunction.

Our study indicates that inhibition of S1PR1 signaling specifically in the endothelium exacerbates BBB dysfunction upon ischemic-hypoxic injury and thereby heightens neuronal injury resulting in worsened neurological outcomes. Given the expression of S1PR1 in the cerebrovascular endothelium in humans and recent findings indicating that S1P-S1PR1 anti-inflammatory signaling in the endothelium could be limiting in cardiovascular disease and other inflammatory conditions, the therapeutic and diagnostic potential of the endothelial sphingosine-1-phosphate pathway in stroke is very high.

INTRODUCTION

The cerebrovascular endothelium, in coordination with pericytes [1, 2] and astrocytes [3] plays a critical role in the maintenance of the blood brain barrier (BBB). BBB dysfunction has been implicated in the exacerbation of neurovascular ischemic, hypoxic and inflammatory injury, which occurs after stroke, a leading cause of mortality and long-term disability worldwide[4]. For instance, the use and effectiveness of current therapies for ischemic stroke (i.e. tissue plasminogen activator, tPA, or mechanical recanalization) are severely limited by the vascular complications of reperfusion injury (i.e. blood brain barrier dysfunction leading to vasogenic edema and hemorrhagic transformation)[5-9]. In hemorrhagic stroke, perihematoma edema volume expansion is associated with worsened outcomes [10]. In subarachnoid hemorrhage (SAH), blood brain barrier breakdown occurs in the acute phase and correlates with more severe neurological deficits [11-13]. However, currently, there are no therapies specifically targeting the endothelium to promote BBB function and prevent exacerbation of neurovascular injury in stroke. A better understanding of the cellular and molecular mechanisms governing BBB function may help design novel therapies aimed at mitigating cerebral endothelial barrier dysfunction in stroke in order to prevent exacerbation of neurovascular injury and improve outcomes.

S1P, a bioactive lipid very abundant in plasma, is a potent modulator of endothelial and lymphocyte function. Plasma S1P originates from endothelial cells[14, 15] and erythrocytes[16] and it is bound to lipoproteins (e.g. HDL[17, 18] via apolipoprotein M (ApoM)[18]), albumin and other chaperones. In mice, S1P signaling via S1PR1 is required for embryonic and postnatal vascular development and maturation in brain and other organs [19, 20 21]. In adult mice, S1PR1 promotes endothelial barrier function, vascular stabilization and inhibits endothelial inflammation [22-24]. These effects are dependent on the activation of anti-inflammatory signaling pathways (Gi- phosphatidylinositol-3-kinase leading to activation of Rac and Akt) which strengthen endothelial barrier function by promoting actin cytoskeleton dynamics (cortical actin assembly) and adherens junctions assembly to the cytoskeleton. In contrast, S1P binding to S1PR2 induces barrier dysfunction and activates pro-inflammatory signaling pathways (e.g. NFκB) in a Rho-Rho kinase dependent way. S1P-S1PR1

antiinflammatory signaling pathway is predominant in the endothelium when S1P is bound to HDL via ApoM [24] (Reviewed in [25]). Indeed, a good part of the cardiovascular protective effects of HDL depend on its content of S1P [26-28] and ApoM [24], which also has been shown to protect plasma S1P from degradation [18]. Recent studies indicate that S1P anti-inflammatory and vasoprotective signaling via S1PR1 could be limiting in human cardiovascular and inflammatory diseases [28-31 25]. For instance, in coronary artery disease, the content of ApoM or S1P in the HDL fraction is significantly reduced, and it inversely correlates with the severity of the disease[28, 29]. In addition, in patients suffering inflammatory conditions such diabetes or sepsis, plasma ApoM levels are significantly decreased compared to control patients [32, 33].

Interestingly, S1PR1 also plays a critical role in lymphocyte trafficking and function[34]. Indeed, the immunosupressor FTY720, which has been approved by the FDA for multiple sclerosis [35, 36], is a S1PR1 functional antagonist (i.e. a potent S1PR1 agonist which induces S1PR1 internalization and degradation [37, 38]). Recent studies attempting to understand the role of S1P in cerebral ischemia have relied on the use of the immunosuppressor FTY720 and other S1PR1 agonists [39, 40, 41 42], which protected in experimental stroke, mainly due to their immunosuppressive effects[42](reviewed in[25]). Thus, these studies could not determine the role of endothelial-specific S1P signaling in BBB function modulation and its impact on brain injury and stroke outcomes. Although immunosuppression is protective in experimental stroke, it is not clear that it could be a good therapeutic strategy in humans, since it increases the risk of developing infections and sepsis, which is an important cause of worsened outcomes and mortality in stroke patients [43, 44]. Hence, a better understanding of the role of endothelial S1P signaling in stroke will be important for future design of novel vasoprotective therapeutic agents targeting this pathway in the endothelium without compromising the immune response.

Given the pathophysiological relevance of the S1P-S1PR1 pathway in humans and in order to bridge this knowledge gap, in this study we aimed to investigate the expression of S1PR1 in the mouse and human brain as well as the role of endothelial-specific S1PR1 signaling in modulation of blood brain barrier function and its impact on brain injury upon subarachnoid hemorrhage, the most

devastating type of stroke. Our results show the critical role of endothelial-specific S1PR1 signaling in BBB function and its impact on stroke outcomes. They also indicate direct causality between endothelial barrier dysfunction and the exacerbation of neuronal injury, highlighting the critical role of the endothelium in the pathophysiology of brain injury and its therapeutic potential.

METHODS

Mice. All animal experiments were approved by the Weill Cornell Institutional Animal Care and Use Committee. Endothelial cell specific *S1pr1* knockout mice (*S1pr1*$^{flox/flox}$*xCdh5–Cre*^{ERT2}*;* referred to as *S1pr1*^{iECKO}) were generated as we have described [45]. *S1pr1*$^{flox/flox}$ mice [20] were crossed to *Cdh5–Cre*^{ERT2} mice [46] to generate *S1pr1*$^{flox/flox}$ *Cdh5-Cre*^{ERT2} mice. Mice were treated with tamoxifen (Sigma-Aldrich) by oral gavage (75 mg kg^{-1}) for 3 days at the age of 8 weeks and used for the experiments 3-4 weeks after tamoxifen treatment. *S1pr1*$^{flox/flox}$ littermates treated with tamoxifen were used as control mice. S1pr1-eGFP knock in mice [47] weighing 26-30 g were used for the expression studies. All experiments were performed in male mice.

Endovascular perforation SAH surgery. SAH surgery was performed on C57/BL6/J, *S1pr1*^{iECKO} mice and their littermate *S1pr1*$^{flox/flox}$ controls as we have previously described [48]. In brief, surgery was performed using a dissecting surgical microscope. Temperature was maintained at 36.5–37.5 °C by using a thermostatic blanket (Harvard Apparatus, CMA 450 Animal Temperature Controller) throughout the procedure. Mice were anesthetized with isoflurane inhalation delivered by facemask in 100% of O_2. A 15 mm midline vertical incision was made on the skin in the head. The head was fixed in stereotactic frame and cerebral blood flow was measured by Laser-speckle imager (PeriCam PSI system, Perimed, Sweden). During surgery, mice were in supine position. A 10 mm midline vertical incision was made on the skin in the neck. The common carotid, external carotid and internal arteries were dissected from the adjacent tissue. The superior thyroid artery and the occipital artery were cauterized and cut. The external carotid artery was sutured with a dead knot and cauterized above the suture. A second suture loop was also placed in the external carotid artery just before the bifurcation of the common carotid artery. A slit-knot was placed around the common carotid artery. A small clip was applied to the internal carotid artery and the slip-knot around the common carotid artery was tightened temporally. A small incision was made in the external carotid artery stump. A 5-0 monofilament with a modified tip (0.28 mm diameter or 0.28 mm x 1.7 mm) was inserted into the incision and the knot around the external carotid artery was tightened to prevent bleeding. Then, the monofilament was advanced to the common carotid artery,

the small clip on the internal carotid artery was removed and the monofilament was guided through the external carotid artery to the internal carotid artery. The knot around the common carotid artery was opened again and the monofilament was introduced to the bifurcation of the internal carotid artery. The monofilament was gently pushed ~1 mm further and then withdrawn to the external carotid artery. The knot around the external carotid artery was loosen and the monofilament was slowly removed. The external carotid artery was quickly ligated to prevent bleeding. The mouse was turned in prone position and induction of subarachnoid hemorrhage was confirmed by reduction of cerebral blood flow by Laser-speckle contrast imager. After the surgery, all animals were maintained in a small animal heated recovery chamber. Two different severities of SAH models were created by changing the tip shapes of a 5-0 monofilament; a rounded tip 0.3mm in diameter was used for mild SAH model, a tip 0.3 mm x 1.7 mm for severe SAH model. The surgeon and the investigator conducting the analysis were blinded to the genotype of the mice. Animals which did not exhibit a reduction in CBF upon endovascular rupture were excluded from the study.

RNA isolation, reverse transcription and quantitative PCR analysis (RT-qPCR)

Total RNA from mouse brains and cells was prepared using RNeasy Mini Kit (Qiagen, Valencia, CA) as instructed by the manufacturer. To generate cDNA, 100 ng of RNA was reverse transcribed using random primers and SuperScript II RT-polymerase (Invitrogen, Carlsbad, CA). Primers were designed using the Primer Express oligo design program software (Applied Biosystems, Foster City, CA). Real-time quantitative PCR was performed using the SYBR Green I assay on the ABI 7500 Sequence Detection System (Applied Biosystems). PCR reactions for each cDNA sample were performed in duplicate and copy numbers were calculated using standard curves generated from a master template as we previously described. The sequence of the primers used for qPCR are shown in Table 2.

S1PR1 Immunohistochemistry

Human tissues were retrieved from Brigham and Women's Department of Pathology archives; this work was approved by the Institutional Review Board (Protocol #2013P001431).

Immunohistochemistry for S1PR1 was performed on an automated stainer (Leica Bond III, Leica

Biosystems, Buffalo Grove, IL) using an anti-human S1PR1 rabbit polyclonal antibody (Santa Cruz Biotechnology Inc.) at a final concentration of 1.3 ug/ml. The IHC technique for S1PR1 was validated as we have previously described [49]. 5μm formalin fixed paraffin embedded tissue sections of human frontal cortex were deparaffinized and processed using heat induced epitope retrieval with an EDTA-based buffer (Leica #AR9640) for 20 minutes and incubated with primary antibody for 30 minutes at room temperature. Secondary antibody (polymer) incubation (10 minutes) and diaminobenzidine-based signal generation (10 minutes) were performed per manufacturer's instructions (Leica # DS9800). Pictures were taken using SPOT Insight Gigabit camera and SPOT Imaging Software (5.1).

Immunofluorescence staining

Under deep anesthesia, mice were perfused with cold PBS and subsequently with 4% PFA in PBS solution. The brains were removed, postfixed with 4% PFA for 24 h, transferred to 30% sucrose solution in PBS, embedded in OCT media and frozen. Coronal sections were cut (30 μm) in a cryostat and immunofluorescence was conducted in floating sections. Sections were preserved at -20^{0}C in a PBS solution containing 30% polyethylene glycol and 30% sucrose. Sections were washed three times with Tris-buffered saline (TBS) and were then blocked with TBS-blocking solution (1 % bovine serum albumin, 0.2 % skim milk, and 0.3 % Triton X-100 in TBS) for 1 h and incubated with the specified primary antibodies in TBS-blocking solution overnight on a shaker at 4 °C, followed by the appropriate secondary antibodies for 2 hours at room temperature. Brain slices were stained with 4',6-diamidino-2-phenylindole (DAPI) for 7 minutes and were mounted onto slides. Samples were observed on a Zeiss LSM 510 Meta Confocal microscope (Carl Zeiss Microscopy, Thornwood, NY). Images were captured using Zen LE software (Carl Zeiss Microscopy).

Isolation of cortical microvessels. The brain microvessels were isolated as we have previously described [50]. All procedures were performed in a cold room. The brains were collected and rinsed in MCDB131 medium (Thermo Fisher Scientific) with 0.5% fatty acid-free BSA (Millipore Sigma). The leptomeninges, cerebellum, brainstem and white matter were removed on ice. The cortices were

homogenized in 8 mL of MCDB131 medium with 0.5% fatty acid-free BSA using a 7-mL loose-fit Dounce tissue grinder (Sigma-Aldrich) with 10 strokes. The homogenates were centrifuged at 2,000 g for 5 min at 4 °C. The pellet was suspended in 15% dextran (molecular weight ~70,000 Da, Sigma-Aldrich) in PBS and centrifuged at 10,000 g for 15 min at 4 °C. The pellet was resuspended in MCDB131 with 0.5% fatty acid-free BSA and centrifuged at 5,000 g for 10 min at 4 °C. The pellet contained the brain microvessels.

Protein extraction from brain microvessels and western blotting. Brain microvascular fragments were lysed in HEPES-RIPA buffer (50 mM HEPES pH 7.5; 1% Triton; 0.5% sodium deoxycholate; 0.1% SDS; 500 mM NaCl; 10 mM MgCl2; 50 mM β-glycerophosphate) with 1x Protease inhibitor cocktail (CalBiochem), 1 mM Na3VO4 and 1 mM NaF and centrifuged at 15,000 r min^{-1} for 15 min. Equal amount of proteins were mixed with SDS sample buffer, boiled and separated on a 4-15% polyacrylamide gel (Bio-Rad), transferred to PVDF membranes (Millipore Sigma), and blocked 5 % milk in 0.1% Tween-20 in TBS. Immunoblot analysis was performed with S1PR1 (1:250; Santa Cruz, cat. no. sc25489) and β-actin (1:1,000; Santa Cruz, cat. no. sc-1616 HRP) antibodies. Membrane were washed with 0.1% Tween-20 in TBS, incubated with anti-rabbit IgG secondary antibody conjugated to horseradish peroxidase (1:2,000; Cell Signaling), and protein bands were visualized with enhanced chemilumescent (ECL) reagent (Thermo Fisher Scientific) on a Protec OPTIMAX X-Ray Film Processor. Relative band intensities were obtained by densitometric analysis of images using ImageJ software.

Brain endothelial cell isolation and assessment of deletion efficiency of endothelial *S1pr1 mRNA*. Two weeks after tamoxifen treatment, mice were sacrificed and the brains were collected and rinsed in MCDB131 medium (Thermo Fisher Scientific) with 0.5% fatty acid-free BSA (Millipore Sigma). The cortices were homogenized in MCDB131 medium using a 7-mL loose-fit Dounce tissue grinder (Sigma-Aldrich) with 15 strokes. The homogenate was mixed with same amount of 30% dextran (molecular weight ~70,000 Da, Sigma-Aldrich) in PBS and centrifuged at 4,500 r min^{-1} for 15 min at 4 °C. The pellet was resuspended in MCD131 medium and centrifuged at 2,400 r min^{-1} for 10 min. The pellet was resuspended in Liberase TM solution (3.5 U; Roche) with DNaseI (0.4 U;

AppliChem Inc) and digested at 37.0 °C for 90 min. The enzymatic reaction was stopped by adding 2 mM of EDTA and 2% of BSA. After centrifugation at 2,400 r min^{-1} for 10 min, the pellet was incubated in purified Rat Anti-Mouse CD31antibody (MEC13.3) (1 : 100; BD Biosciences) with Dynabeads Sheep Anti-Rat IgG (Invitrogen, cat. no. 11035) for 35 min. CD31 positive endothelial cells were isolated by using DynaMag-2 Magnet (Thermo Fisher Scientific). Total RNA was extracted from the isolated endothelial cells using shredder (Qiagen) and RNeasy Mini Kit (Qiagen) with RNase-free DNase treatment (Qiagen) according to the manufacturer's instructions. Reverse transcription was carried out using Verso cDNA Synthesis Kit (Thermo Fisher Scientific). Real-time PCR was performed on a real-time PCR system (Applied Biosystems, ABI 7500 Fast) by using PerfeCTa SYBR Green Fast Mix Low ROX. PCR primer sequences for target molecules are in Table 2.

Grading system for SAH. Blood volume in the subarachnoid space was assessed using the grading system previously reported [51]. Mice were sacrificed under deep anesthesia 24 h after SAH induction and the brains were removed. Pictures of ventral surface of the brain depicting the basal cistern with the circle of Willis and the basilar artery were taken using a stereomicroscope (Olympus, SZX16) equipped with digital camera (Olympus, DP12). The basal cistern was divided into 6 segments and a grade from 0 to 3 was given to each segment: Grade 0, no subarachnoid blood; Grade 1, minimal subarachnoid blood; Grade 2, moderate blood clot with recognizable arteries; Grade 3, blood blot obliterating all arteries. Blood volume was evaluated by a total score ranging from 0 to 18 from six segments.

Tail bleeding assay. Tail bleeding time was determined as described previously[52]. A mouse was anesthetized with a mixture of ketamine and xylazine, and body weight was measured. The mouse was placed on a heating pad in prone position, the tail tip was about 4 cm blow the body horizon. A distal 5 mm segment of the tail was amputated, and the tail was immediately immersed in PBS pre-warmed at 37 °C. The time to complete arrest of bleeding was determined: complete arrest is no blood flow for 1 minute. The blood volume was determined by hemoglobin assay. Blood cells were separated by centrifuge at 4,000 r/min for 5 min at room temperature, and erythrocytes were

resuspended in BD Pharm Lyse (BD Biosciences). After 10 min incubation in the buffer, the lysate was centrifuged at 10,000 rpm/min for 5 min. Hemoglobin concentrations were measured spectrophotometrically at 550 nm using a plate reader (Molecular Devices, SpectraMax M2e).

Mortality and neurological outcome. Mortality was assessed at 24, 48 and 72 hours after SAH induction. Gross neurological outcome was blindly evaluated before and at 24, 48 and 72 hours after surgery by sensorimotor scoring as described previously [53, 54]. Briefly, a motor score (0 to 12; spontaneous activity, limb symmetry, climbing, and balance) and a sensory score were used. Gross neurological outcome was evaluated by a total score of 4 to 24. Higher scores indicate better neurological outcome.

Brain water content. Brain edema was determined by using the wet/dry method as previously described [55]. Mice were sacrificed at 72 hours after surgery and the brains were quickly removed and separated into the left and right cerebral hemispheres and weighed (wet weight). The brain specimens were dried in an oven at 55°C for 72 hours and weighed again (dry weight). The percentage of water content was calculated as ([wet weight-dry weight]/wet weight) x 100%.

Cell death detection. DNA strand breakage during apoptosis after SAH was assessed by phospho-histon H2A.X (Ser 139) immunofluorescence as previously described [56]. Because phosphorylation of histon H2A.X at Ser 139 (γ-H2AX) is abundant, fast, and correlates well with each DNA strand breakage, it is the most sensitive marker that can be used to examine the DNA damage [57]. Mice were deeply anesthetized and perfused with cold PBS and subsequently with 4% PFA in PBS solution. The brains were removed, post-fixed with 4% PFA for 24 h and transferred to 30% sucrose solution. Frozen brains were cut with a 10 μm of thickness by a cryostat (Leica, CM3050 S). The brain slices were blocked with TBS- blocking solution (5% bovine serum albumin and 0.5% Tween 20 in PBS) for 1 hour at room temperature and incubated with phospho-histone H2A.X (Ser 139) (20E3) antibody (1:100; Cell Signaling) in blocking solution overnight on a shaker at 4 °C. Sections were washed three times with 0.5% Tween 20 in PBS and then incubated with goat anti- rabbit IgG Alexa- 488 (1:200; Life Technologies, cat. no. A-11008). DAPI (40 ,6-diamidino-2-phenylindole) staining was used as a counter staining. Sections were imaged by using

an FluoView FV10i confocal microscope (Olympus, Japan) (original magnification, x 40). For quantification, the percentage of phospho-histon H2A.X positive cells per DAPI positive cells from three different fields in the ipsilateral cerebral cortex area per mouse (bregma -1.64 to -1.28 mm) were counted and the average values were plotted.

Assessment of blood brain barrier dysfunction. Small molecule (≤ 3 kDa) leakage from the blood into the brain parenchyma was assessed using dextran–tetramethylrhodamine (TMR) (3-kDa) dye (Thermo Fisher Scientific) Dextran-TMR (3-kDa) extravasation experiments were performed as described with modifications [2, 45, 58]. Mice were anesthetized and Dextran-TMR (3-kDa) (10 μg g^{-1}) was injected in the external jugular vein 22 hours after surgery. After 2 hours circulation, mice were deeply anesthetized and perfused with cold PBS to remove intravascular dye. The ipsilateral hemispheres were removed and homogenized in 1% Triton X-100 in PBS. The lysate was centrifuged at 15,000 r min^{-1} twice for 15 min at 4 °C, and the supernatant was used to measure fluorescence (excitation/ emission = 540/590 nm, SpectraMax M2e, Molecular Devices). The relative fluorescence values (R.F.U.) were normalized by the brain weights.

To assess albumin extravasation, evans blue dye (EBD) was used because EBD binds to plasma albumin[59]. Mice were anesthetized and 2% EBD (4 ml kg^{-1}) was injected in the external jugular vein 21 hours after surgery. After 3 hours circulation, mice were deeply anesthetized and perfused with cold PBS to remove intravascular dye. The ipsilateral hemispheres were removed and homogenized in 50% trichloroacetic acid in PBS. The lysate was centrifuged at 15,000 rpm min^{-1} twice for 15 min at 4 °C, and the supernatant was used to measure fluorescence (excitation/ emission = 620/680 nm, SpectraMax M2e, Molecular Devices). The relative fluorescence units (R.F.U.) were normalized by the brain weights.

Statistical analysis. All results were expressed as mean ± SEM. Statistical analysis were performed with GraphPad Prism (GraphPad Software, Version 7.0c) by using two-tailed Student's t-test, one-way analysis of variance (ANOVA) followed by Tukey's test or two-way ANOVA followed by Bonferoni's test. *P* values < 0.05 were considered statistically significant.

RESULTS

Abundant expression of S1PR1 in the mouse and human brain

We first investigated the expression of S1PR in brain, mouse primary neurons and mouse brain endothelial cells by reverse transcription and quantitative PCR analysis (RT-qPCR), as we have previously described [49, 60]. We found that S1PR1 is robustly expressed in the mouse brain *in vivo*, (Fig. 1A, 20.5± 2.4 copies/10^6 18S, which is equivalent to approximately 20.5± 2.4 S1PR1 mRNA copies/cell [61]), as well as in the mouse brain endothelial cell line bEnd.3 [62] (Fig. 1B, 87.3±2.9 copies/cell), mouse primary neurons (Fig. 1C, 16.4±1.3 copies/cell) and mouse primary mixed glial cells (Fig. 1D, 8.3±0.15 copies/cell) *in vitro.* Then, we compared the expression of S1PR1 in cortical microvessels fragments[45] to its expression in total brain. Interestingly, we found that S1PR1 transcripts are highly enriched in cortical microvessels when compared to total brain (Fig. 1E, ~6 fold enrichment in microvessels *vs* whole brain).

Using the S1pr1-eGFP knock in mice, in which endogenous S1PR1 has been replaced by the S1PR1-eGFP fusion protein [47], we found that S1PR1 is abundantly expressed in the cerebrovascular endothelium all throughout the brain (Fig. 2A, B, representative pictures from corpus callosum and cortex) as assessed by detection of S1PR1-eGFP and immunofluorescence (IF) analysis for the glucose transporter 1 (Glut-1). S1PR1 is also expressed in cortical (Supplementary Figure 1A) and hippocampal (Supplementary Figure 1B) neurons (co-staining with MAP-2) *in vivo*, both in the neuronal soma and the neuropil. In addition, S1PR1-eGFP is expressed in some GFAP positive cells, indicating that S1PR1 is also expressed in astrocytes (Supplementary Figure 1C, D). Similar pattern of expression was observed in the mouse brain when immunofluorescence analysis was conducted using a S1PR1 specific antibody previously validated in our laboratory [49] (data not shown).

In order to investigate the expression of S1PR1 in the human brain, we conducted IHC analysis in sections from the frontal lobe of a total of 5 brain autopsy samples. The S1PR1 antibody and IHC protocol used in human samples were previously validated in our laboratory [49]. We observed a very similar pattern of S1PR1 detection in these 5 samples. Representative pictures of the frontal cortex

are shown in Figure 3. S1PR1 immuno positivity was observed both in the grey matter (GM) and white matter (WM) areas (Figure 3A, low magnification). S1PR1 was widely detected in the cerebrovascular endothelium of parenchymal vessels (in the grey matter and white matter, Fig. 3B, D-F) and pial vessels (Fig. 3C). In the grey matter, S1PR1 staining was observed in neuronal bodies and in the neuropil (Fig. 3B, C).

Altogether, our data indicate that, S1PR1 is the most abundant S1PR transcript in brain, brain endothelial cells and neurons. S1PR1 protein is also widely detected in the mouse and human brain, in the cerebrovascular endothelium and neurons. S1PR1 mRNA is highly enriched in mouse cerebral microvessels when compared to total brain.

Lack of S1pr1 in the endothelium results in worsened outcomes in the acute phase of SAH

In order to investigate the role of endothelial S1PR1 signaling in the pathophysiology of aneurysmal SAH, we used the endovascular rupture model of SAH[48], which is a well established and reproducible model that recapitulates key features of the pathophysiology of the acute phase of SAH. 24, 48 and 72 hours after SAH, cerebral microvessels were isolated from the mouse cortex of wild type mice to determine sphingosine 1-phosphate receptor 1 (S1PR1) mRNA and protein levels compared to sham mice. We found that S1PR1 mRNA levels in cortical microvessels did not significantly change compared to sham animals at 24, 48 or 72 h after SAH (Fig. 4A). Gfap mRNA levels in microvessels, which is induced in astrocytes upon inflammation, were significantly higher after SAH compared to sham (Fig. 4B, 3.07 ± 0,1, 4.05 ± 0.39 and 3.4 ± 0.56 fold induction at 24, 48 and 72 h respectively). The levels of endothelial (ZO-1, Fig. 4C), pericyte (CD13, Fig. 4D) or astrocyte end foot (Aqp4, Fig. 4E) markers did not significantly change suggesting similar cell composition among the microvessel preparations from these groups of mice. S1PR1 protein was widely detected by western blot assay in cerebral microvessels in sham animals (Supplementary Figure 2). Only a very modest increase in S1PR1 protein at 24 hours after SAH was observed (1.68 ± 0.19-fold). These data indicate that, in the acute phase of SAH, neurovascular inflammation is induced, assessed by increased GFAP expression (3-4 fold induction) but there were no significant

changes in S1PR1 mRNA levels in cerebral microvessels. Only a modest increase in S1PR1 protein levels was observed 24 hours after SAH.

Given the abundant expression of S1PR1 in the cerebrovascular endothelium in the mouse and human brain, and the enrichment in S1PR1 mRNA in mouse cortical microvessels compared to total brain, we aimed to investigate the role of endothelial S1PR1 in early brain injury (EBI) after SAH. We generated endothelial-specific S1PR1 null mice (S1PR1 ^{iECKO}) by treating adult *S1pr1*$^{flox/flox}$*xCdh5–Cre*^{ERT2} mice (~2 month old) with 75 mg kg^{-1} tamoxifen for 3 consecutive days (Fig.4F) as we have recently described[45]. *S1pr1*$^{flox/flox}$ littermate mice were also treated with tamoxifen and used as wild type control. We assessed the efficiency of deletion in S1PR1^{iECKO} by isolating brain endothelial cells from mice 2 weeks after tamoxifen treatment. RT-qPCR analysis demonstrated ~90% reduction of *S1pr1* expression in *S1pr1*^{iECKO} mice compared to *S1pr1*$^{flox/flox}$ littermate mice treated with tamoxifen in the same manner (Fig. 4F).

S1pr1^{iECKO} and *S1pr1*$^{flox/flox}$ littermate mice were subjected to SAH surgery using a modified 5.0 suture (0.28 mm x 1.7 mm) to induce severe SAH as described in the method section [48]. The mortality rates were 10% in *S1pr1*$^{flox/flox}$ mice at day 1, 2 and 3 after SAH. Interestingly, the mortality rates in endothelial-specific S1PR1 null mice (*S1pr1*^{iECKO} mice) were significantly higher compared to wild type (*S1pr1*$^{flox/flox}$,40% at day 1, and 60% at day 2 and 3, Fig. 4G).

Due to the higher mortality rates in *S1pr1*^{iECKO} *mice, S1pr1*$^{flox/flox}$ and *S1pr1*^{iECKO} *mice* were subjected to a milder SAH model by changing the shape of the tip of the nylon suture to perforate the cerebral artery (0.28 mm diameter, as described in methods section) *S1pr1*^{iECKO} mice exhibited a trend towards a higher mortality rate (26.3% in day 1, 2 and 3) compared to *S1pr1*$^{flox/flox}$, which exhibited a mortality rate of 7.7% at day 1, 2 and 3(Fig. 4H), although it was not statistically significant. Given the high mortality rate in *S1pr1*^{iECKO} subjected to the severe SAH model (Fig. 4G), we used the milder SAH model for subsequent studies.

These data indicate that endothelial specific deletion of S1PR1 in mice results in a dramatic increase in mortality rates in the acute phase of SAH.

Genetic deletion of *S1pr1* in the endothelium has no effect on hemostasis, blood volume in the subarachnoid space or CBF changes after SAH.

Since the volume of subarachnoid blood directly correlates with worse outcomes after SAH [63 51], we quantified the amount of subarachnoid blood upon SAH in *S1pr1*^{iECKO} and *S1pr1*$^{flox/flox}$ mice by image analysis using a previously described SAH grading system [51]. No significant differences were observed in the amount of subarachnoid blood between *S1pr1*$^{flox/flox}$ and *S1pr1*^{iECKO} mice 24h after SAH (Fig. 5A, representative pictures). SAH grading was 11.50 ± 0.62 in *S1pr1*$^{flox/flox}$ mice and 11.67 ± 0.42 in *S1pr1*^{iECKO} (Fig. 5B). In addition, we determined hemostasis using the tail bleeding assay [52]. Consistent with the subarachnoid blood data, we did not find any significant differences in the bleeding times or blood volumes between *S1pr1*$^{flox/flox}$ and *S1pr1*^{iECKO} mice in the tail bleeding assay. Bleeding times were 68.88 ± 4.98 seconds in *S1pr1*$^{flox/flox}$ and 63.8 ± 4.14 seconds in *S1pr1*^{iECKO} (Fig. 5C). Hemoglobin contents, assessed by measuring the absorbance at 550 nm, were 0.73 ± 0.07 in *S1pr1*^{iECKO} mice compared to 0.70 ± 0.12 in *S1pr1*$^{flox/flox}$ mice (Fig. 5D). Altogether these data indicate that hemostasis is not impaired in *S1pr1*^{iECKO} mice compared to wild type mice and that the amount of blood in the subarachnoidal space upon SAH is similar in wild type and *S1pr1*^{iECKO} *mice.*

We also determined cerebral blood flow (CBF) changes during SAH in both groups of mice by Laser-Speckle flowmetry. Cerebral blood flow in the middle cerebral artery (MCA) territory rapidly dropped ~1 minute after SAH in both the ipsilateral side (to 31.65 ± 3.46% of basal in *S1pr1*^{iECKO} and to 40.26 ± 4.09% of basal in *S1pr1*$^{flox/flox}$) and the contralateral side (to 82.42 ± 3.72% of basal in *S1pr1*^{iECKO} and to 77.32 ± 3.90% of basal in *S1pr1*$^{flox/flox}$). Then, CBF recovered to ~85% of basal 2 h after SAH in the ipsilateral side (to 87.46 ± 7.15% in *S1pr1*^{iECKO} versus to 82.83 ± 5.88% in *S1pr1*$^{flox/flox}$) and ~95 to 100% in the contralateral side (102.81 ± 1.97% in *S1pr1*^{iECKO} versus 95.34 ± 4.86% in *S1pr1*$^{flox/flox}$) both in *S1pr1*^{iECKO} and *S1pr1*$^{flox/flox}$ mice (Fig. 5E). These data indicate that genetic deletion of *S1pr1* in the endothelium did not significantly impact CBF changes during SAH.

Finally, no significant differences were observed in arterial O_2 saturation, heart rate, pulse distention (a surrogate of pulse pressure) and respiratory rate between *S1pr1*^{iECKO} and *S1pr1*$^{flox/flox}$ mice, before or after SAH (Table 1).

Altogether, these data indicate that endothelial-specific deletion of S1PR1 in adult mice did not have a significant impact on bleeding or clearance of subarachnoid blood, cerebral blood flow changes or systemic physiological parameters such as heart rate, respiratory rate, O_2 saturation or pulse distension.

Endothelial deletion of *S1pr1* exacerbates brain edema and cell death after SAH leading to worsened neurological outcomes.

In order to determine the impact of the lack of endothelial S1PR1signaling on brain injury after SAH, we assessed brain edema at 72 hours after mild SAH surgery by quantifying total brain water content. *S1pr1*$^{flox/flox}$ mice exhibited a statistically significant increase in brain water content in the ipsilateral hemisphere (82.83 ± 0.53%) compared to sham (81.34 ± 0.20%) (Fig. 6A). Interestingly, in *S1pr1*^{iECKO} mice, total brain edema in the ipsilateral hemisphere was significantly exacerbated (84.39 ± 0.91%) compared to *S1pr1*$^{flox/flox}$ (Fig. 6A). There was no increase in brain water content in contralateral hemisphere compared to sham.

Next, we analyzed cell death at 24 hours after SAH using phospho-histone H2A.X (Ser 139) immunostaining, a marker for DNA fragmentation resulted from apoptosis. We found that *S1pr1*^{iECKO} mice showed significantly higher number of phospho-histone H2A.X positive cells compared to *S1pr1*$^{flox/flox}$ mice (50.85 ± 2.56% in *S1pr1*^{iECKO} versus 34.00 ± 2.98% in *S1pr1*$^{flox/flox}$) (Fig. 6B and C). No apoptotic cells were detected in sham animals.

Finally, we aimed to determine the impact of genetic deletion of S1PR1 in the endothelium on neurological outcomes after SAH. Neurological outcomes were determined by assessing motor and sensory function using a total scale of 4 to 24 (being 24 the best neurological outcome) as previously described[53, 54]. Neurological outcomes at 24h and 48h after mild SAH surgery were worsened in *S1pr1*^{iECKO} mice (16.29 ± 1.37 and 17.14 ± 1.40, respectively) compared to *S1pr1*$^{flox/flox}$ mice (20.91 ± 0.81 and 21.00 ± 0.83, respectively) (Fig. 6D).

These data indicate that genetic deletion of *S1pr1* specifically in the endothelium significantly exacerbates total brain edema and cell death resulting in poorer neurological outcomes.

Endothelial specific deletion of *S1pr1* in adult mice exacerbates blood brain dysfunction after SAH.

Disruption of the BBB is an early event in the pathophysiology of neurovascular ischemic and hypoxic injury. Two distinct cellular mechanisms of BBB dysfunction have been described. Endothelial transcytosis [64] (i.e. the transcellular pathway) [2] allows the passage of high molecular weight molecules (e.g. albumin). In addition, small molecules can leak through the intercellular junctions (tight and adherens junction proteins, i.e. paracellular pathway) [58, 64-67]. In order to quantify BBB dysfunction upon SAH, we used two different tracers: Evans blue dye, which binds to plasma albumin (~66 kDa), and thus given its bigger size, it can leak into the brain parenchyma via transendothelial vesicle trafficking [64] or after a severe loss of vascular integrity; tetramethylrhodamine (TMR)-labeled 3-kDa dextran which, due to its small molecular weight tracer can cross the BBB via the intercellular junctions (paracellular pathway) [2, 58].

24 hours after SAH, albumin leakage, assessed by EBD extravasation assay, was significantly increased in *S1pr1*$^{flox/flox}$ mice compared to sham animals (Fig 7A, 1.53 ± 0.06 fold in *S1pr1*$^{flox/flox}$ SAH versus *S1pr1*$^{flox/flox}$ sham). Albumin extravasation 24 after SAH was significantly higher in *S1pr1*^{iECKO} mice with regards to *S1pr1*$^{flox/flox}$ (1.83 ± 0.08 in *S1pr1*^{iECKO}, Fig. 7A). Sham *S1pr1*^{iECKO} mice did not exhibit increased albumin leakage compared to sham wild type *S1pr1*$^{flox/flox}$ litter mates (Fig. 7A). However, they did exhibit small molecule (3KDa TMR-dextran) BBB leakage (2.87 ± 0.45 fold in sham *S1pr1*^{iECKO} compared to sham *S1pr1*$^{flox/flox}$, Supplementary Fig. 3), consistent with our recently published studies [45].

Mechanistically, we found that exacerbated BBB dysfunction in endothelial-specific S1PR1 null mice, correlated with increased phosphorylation of myosin light chain (MLC) in isolated cortical microvessels (Fig. 6B, 6.96±1.6 fold in *S1pr1*^{iECKO} *versus S1pr1*$^{flox/flox}$), a downstream effector of the

Rho-ROCK pathway implicated in endothelial inflammation and blood brain barrier dysfunction [58, 68-70].

These data indicate that BBB dysfunction after SAH (albumin leakage) is heightened in mice lacking S1PR1 specifically in the endothelium compared to wild type and correlates with increased phosphorylation of MLC.

DISCUSSION

Increasing preclinical and clinical evidence indicate that BBB dysfunction correlates with exacerbated neuronal injury and plays a critical role in the pathophysiology of ischemic, hypoxic and inflammatory neurovascular injury in stroke [5-13], traumatic brain injury[71 72, 73] and other acute[74, 75] and chronic [76-79]clinical conditions. Novel strategies to prevent BBB dysfunction may help minimize exacerbation of neuronal injury in these clinical settings. While the therapeutic potential of the endothelium is beginning to be recognized [25, 80, 81], yet much research is needed to better understand the endothelial molecular mechanisms involved in the modulation of BBB function in these conditions.

Aneurysmal SAH, the most devastating type of stroke, occurs when an intracranial aneurysm ruptures. Compared to other types of stroke, SAH occurs earlier in life (40-60 years)[82] and leads to higher mortality (50%) [83]. In addition, SAH survivors experience a high degree of disability and cognitive impairment (memory, language and executive function) [84] with personal and societal consequences. SAH causes transient cerebral ischemia and accumulation of blood in the subarachnoid space, leading to brain injury, BBB dysfunction, cytotoxic and vasogenic cerebral edema in the acute phase [12, 85, 86]. Although numerous studies have reported the direct correlation between endothelial barrier dysfunction and worsened SAH outcomes in humans [87, 88] and mice [86, 89-94], no direct causality regarding the contribution of BBB dysfunction to the exacerbation of neuronal injury has been shown. In this study, we investigated the role of the endothelium and BBB dysfunction in the aggravation of brain injury in the acute phase of SAH by using a well-established mouse model of aneurysmal SAH, the endovascular rupture model [48]. This experimental model faithfully recapitulates key features of the acute phase of SAH: upon rupture of the MCA, blood pours into the subarachnoid space, increasing intracranial pressure which gives rise to a brief period of transient (~3-5 minutes) cerebral ischemia [48] (Fig. 5E, ~70%reduction of CBF in ipsilateral hemisphere). CBF slowly recovers over the time, but the brain remains hypoperfused in the acute phase of SAH (Fig. 5E, ~30% reduction vs basal). BBB breakdown, cerebral edema and neuronal injury ensue [89, 92]. In our study, we show that endothelial-specific genetic deletion of S1PR1 in adult

mice exacerbates cerebral edema and neuronal injury, resulting in worsened outcomes in the acute phase of SAH. Thus, our study demonstrates the critical role of the endothelium in SAH outcomes and underscores the importance of a better understanding of the signaling pathways governing BBB function in the design of future therapeutic strategies targeting the endothelium to prevent the exacerbation of brain injury in this devastating condition.

S1P signaling via S1PR1 plays a critical role in endothelial function in humans and mice (reviewed in [25]). Activation of S1PR1 by S1P in the HDL fraction accounts for an important part of the cardiovascular protective effects of HDL[24, 27-29]. S1PR1 also plays a critical role in lymphocyte function: mice lacking S1PR1 in hematopoietic cells are lymphopenic due to impaired egress from thymus and lymphoid organs[34]. Interestingly, the immunosupressor FTY720-P, which has been approved by the FDA for multiple sclerosis [35, 36], is a S1PR1 potent agonist. Given the phenotype of the mice lacking S1PR1 in hematopoietic cells[34] and *in vitro* studies which indicate that FTY720-P induces desensitization of S1PR1 [37, 38] it is accepted that FTY720-P, as well as other agonists [95, 96] and antagonists [97] of S1PR1 lead to immunosuppression via inhibition of S1PR1 signaling. In experimental stroke, FTY720 and S1PR1 specific agonists, as other immunosuppressor drugs, have been shown to be protective[39, 40 41, 42] and have even been tested in pilot stroke clinical trials [98-100]. Although the mechanisms are not completely clear, FTY720 protection has been attributed to its immunosuppressive effects [42] and its ability to desensitize S1PR1. Thus, the role of endothelial specific S1PR1 signaling in BBB function and stroke outcomes had remained elusive. We sought to address this knowledge gap by inducing the deletion of S1PR1 in adult mice, specifically in the endothelium [46] and directly testing the role of endothelial S1PR1 signaling in BBB function and its impact on early brain injury upon SAH. Our data demonstrate that endothelial specific deletion of S1PR1 in adult mice exacerbates neuronal injury and worsens neurological outcomes in the acute phase of SAH, indicating that endothelial S1P signaling via S1PR1 is an endogenous protective signaling pathway that mitigates neurovascular ischemic/hypoxic/inflammatory injury**.** These data are consistent with previous studies from our laboratory and others which indicated that FTY720 exerts agonistic activity for S1PR1 in the endothelium and promotes endothelial barrier function [23,

[25]. Overall, our findings with the endothelial-specific S1PR1 mice highlight the therapeutic potential of this endothelial pathway in stroke. Novel future strategies to target this pathway specifically in the endothelium without compromising the immune response hold promise as novel vasoprotective therapeutic agents in stroke.

Mechanistically, we found that endothelial deletion of S1PR1 exacerbates BBB dysfunction (albumin leakage) upon SAH. BBB dysfunction heightens neurovascular injury by various mechanisms such as by allowing the entrance of neurotoxic plasma components into the brain parenchyma (e.g. albumin [101], fibrinogen [102]) and by compromising the ability of cerebral capillaries to deliver oxygen and nutrients to the neurons [7-9, 103]. In homeostatic conditions, the cerebrovascular endothelium, in cooperation with pericytes and astrocytes maintain a physical, metabolic and transport barrier to restrict the passage of molecules into the brain parenchyma [3, 104, 105]. In contrast to other organs, endothelial transcytosis (i.e. transcellular permeability) is very low in the brain[106]. Crosstalk between the cerebrovascular endothelium and pericytes plays an important role in the inhibition of endothelial vesicular trafficking and expression of leukocyte adhesion molecules at the blood brain barrier [2 107]. In addition, the presence of tight junction proteins is also critical to maintain this physical barrier. Upon ischemic or hypoxic injury, BBB dysfunction starts early, primarily due to two cellular mechanisms, transcellular and paracellular permeability. The induction of gelatinase activity in cerebral microvessels [86, 92, 93, 108-111] leads to basal lamina degradation [7, 112]. In addition, pericyte and endothelial activation gives rise to increased endothelial transcytosis (transcellular permeability)[2, 107], allowing the passage of plasma proteins (e.g. albumin) into the brain parenchyma. Small plasma molecules can also leak via the intercellular junctions (i.e. paracellular permeability) [58, 64], which become weakened by post-translational modifications (e.g. phosphorylation) and their disassembly from the actin cytoskeleton [113]. With regards to molecular mediators and the signaling pathways governing these cellular processes leading to BBB dysfunction, generation of reactive oxygen species [114], NF-κB-mediated induction of MMP-9 [108, 115], VEGF-induced increased vesicular trafficking and junctional destabilization [116, 117], activation of Rho-ROCK pathway [58, 70] and increased angiopoietin 2/1 ratio [118] among others, have been proposed.

We recently reported that endothelial deletion of S1PR1 in adult mice results in a defect in the assembly of tight junctions with the cytoskeleton in cerebral microvessels leading to BBB leakage of small molecules via the intercellular junctions (paracellular route) [45]. Interestingly, in healthy, non-challenged mice, this small molecule BBB leakage induced by endothelial deletion of S1PR1 in adult mice does not result in neuroinflammation or neurological deficits [45]. However, upon SAH challenge, BBB dysfunction (albumin leakage) and neurovascular injury were exacerbated in mice lacking S1PR1 specifically in the endothelium. At the molecular level, exacerbated BBB dysfunction in S1PR1 endothelial specific mice correlated with increased levels of phosphorylated MLC, a downstream effector of the Rho-ROCK pathway implicated in endothelial inflammation and blood brain barrier dysfunction [58, 68-70]. These data indicate that in endothelial S1pr1 null mice, increased p-MLC levels, possibly due to exacerbated Rho/ROCK signaling, correlates with the aggravation of BBB dysfunction and worsened outcomes upon SAH.

Other possible vascular mechanisms responsible for the worsened outcomes in endothelial specific S1pr1iECKO mice vs wild type could be differences in cerebral blood flow or in bleeding upon cerebral artery rupture. However, we did not observe differences in the CBF changes or physiological parameters during and after SAH between these two groups of mice. In addition, the amount of blood in the subarachnoidal space (SAH grade), which plays an important role in the severity of brain injury and SAH outcomes was similar in both groups of mice, indicating that there were no differences in bleeding or the clearance of the subarachnoidal blood. Furthermore, there were no differences in platelet function, assessed by the tail-bleeding assay, between wild type and S1pr1iECKO mice. Thus, the exacerbation of neuronal injury upon SAH in the endothelial specific s1pr1 null mice vs wild type cannot be attributed to differences in bleeding or in cerebral blood flow regulation. Altogether our data points to exacerbation of BBB dysfunction (albumin leakage) as the main cellular mechanism underlying the aggravation of brain injury upon endothelial deletion of S1PR1 in the adult mice, providing proof of concept of the critical role of endothelium and blood brain barrier dysfunction in the aggravation of brain injury in stroke.

Lastly, our study also underscores the pathophysiological relevance of the S1P pathway in

humans. Using RT-qPCR in combination with mouse genetic approaches and IHC techniques previously validated in our laboratory [49], we found that S1PR1 is the most abundant S1PR transcript in the mouse brain and mouse brain microvessels and widely detected in the human cerebrovascular endothelium and brain parenchyma. Our human data, together with our mouse studies using the endothelial-specific S1PR1 null mice, highlight the therapeutic and prognostic potential of the endothelial S1P pathway in stroke. Given recent human studies which indicate that S1P-S1PR1 vasoprotective signaling [24, 27] may be limiting in cardiovascular and inflammatory diseases [25, 28-31] our present data imply that patients with lower levels of ApoM or HDL-bound S1P and thus, having limiting endothelial S1PR1 antiinflammatory signaling, could be at risk of worsened outcomes upon stroke. In addition, our data could help explain the adverse effects reported in some subsets of multiple sclerosis patients in chronic treatment with FTY720, such as macular edema or posterior reversible encephalopathy syndrome, among others [119-122].

In summary, our study demonstrates the critical role of the endothelial-specific S1PR1 signaling in BBB function and SAH outcomes in mice. Our human data strengthen the pathophysiological relevance of these findings and highlight the therapeutic and prognostic potential of the endothelium, more specifically the endothelial S1P signaling pathway in stroke. New strategies to modulate S1P signaling specifically in the endothelium to prevent exacerbation of brain injury without compromising the immune response [25, 123, 124] could hold promise as novel neurovascular protective therapies in stroke and other conditions associated with BBB dysfunction.

ACKNOWLEDGEMENTS

This work was supported by internal funds provided by the Departments of Surgery and Emergency Medicine, Beth Israel Deaconess Medical Center, the Department of Pathology and Laboratory Medicine, Weill Cornell Medicine, American Heart Association Grant-in-Aid 12GRNT12050110, NIH HL094465 and Leducq Foundation grants to TS.

We would like to thank Dan Li and Dr. Shou-ching Jaminet from the Multi-Gene Transcriptional Profiling Core Facility (Center for Vascular Biology Research, Beth Israel Deaconess Medical Center, Harvard Medical School) for the quantitative PCR analysis, Drs. Louise McCullough (University of Texas Health McGovern Medical School) and Tim Hla (Boston Children's Hospital) for their input in the project.

The authors declare no competing financial or non-financial interests.

FIGURE LEGENDS

Figure 1. S1PR1 mRNA is the most abundant S1PR transcript in brain, brain endothelial cells and neurons and it is highly enriched in brain microvessels. S1PR mRNA levels in A) normal mouse brain, B) the mouse brain endothelial cell line bEnd.3, C) primary mouse neurons and D) primary mouse mixed glial cells. E) Comparison of S1PR1 mRNA levels in whole brain versus brain microvessels. Quantitative reverse transcription and polymerase chain reaction (RT-qPCR) demonstrates that S1PR1 transcript is predominant over the other S1PR and it is highly expressed in brain microvessels. B) Log scale. The individual values and the mean ± SEM are shown. N=3-6. *$p<0.05$.

Figure 2. S1PR1 expression in the mouse brain in S1PR1-eGFP knock in mice. S1PR1-eGFP fluorescence confocal analysis in the mouse brain. A-C) S1PR1-eGFP is expressed in the cerebrovascular endothelium. Immunofluorescence for Glut-1 (endothelial marker) is shown in the red channel. Two representative areas from the corpus callosum (A) and cortex (B, C) are shown. C) Selected region from B. Scale bar 20μm. Arrows point to endothelial cells with the brightest green signal. Representative pictures are shown. N=5-6.

Figure 3. S1PR1 expression in the human brain. Representative images of S1PR1 immunohistochemistry in 5 human brain autopsy samples. Formalin-fixed paraffin-embedded tissue sections were used for immmunohistochemical staining of S1PR1, as described in the Methods section. A) Expression of S1PR1 in the white and grey matter. Scale bar 500 μM. B) Representative picture showing S1PR1 immunopositivity in the neuropil, arterioles and capillaries of the grey matter. C) Detection of S1PR1 in the cerebrovascular endothelium of pial vessels. D-F) Representative pictures of the white matter. Notice S1PR1 positivity in parenchymal arterioles (D, F), venules (E) and capillaries (E,F). B-F) Scale bar 50 μM.

Figure 4. Increased mortality and worsened outcomes after SAH in endothelial specific S1pr1 null mice. A-E) S1PR1, GFAP, ZO-1, CD13 and AQP4 mRNA levels in cerebral microvessels were quantified by RT-qPCR. F) *S1pr1*$^{flox/flox}$ and *S1pr1*^{iECKO} mice were treated with tamoxifen (75 mg kg^{-1}) for the consecutive 3 days at the age of 8 weeks. *S1pr1* mRNA expression

levels were analyzed by qPCR in brain endothelial cells isolated from *S1pr1*$^{flox/flox}$ and *S1pr1*^{iECKO} mice 2 weeks after tamoxifen treatment (*n* = 4). Deletion efficacy of endothelial specific *S1pr1* in *S1pr1*^{iECKO} is shown relative to *S1pr1*$^{flox/flox}$ mice. $^{**}P < 0.01$, Student's t-test. G) Survival curves after severe SAH surgery in *S1pr1*$^{flox/flox}$ and *S1pr1*^{iECKO} mice (*n* = 10). H) Survival curves after mild SAH surgery *S1pr1*$^{flox/flox}$ and *S1pr1*^{iECKO} mice (*n* = 13 or 19). G and H) Log-rank test, $^{*}P < 0.05$. Individual values and mean ± s.e.m are shown. $^{*}P < 0.05$, $^{**}P < 0.01$, One-way ANOVA followed by Tukey's test. Red line, *S1pr1*^{iECKO}; Blue line, *S1pr1*$^{flox/flox}$.

Figure 5. Subarachnoid blood volume, hemostasis and CBF changes after SAH in *S1pr1*$^{flox/flox}$ and *S1pr1*^{iECKO} mice. A) Representative images of the ventral side of the brain depicting the basal cistern from *S1pr1*$^{flox/flox}$ and *S1pr1*^{iECKO} mice at 24 hours after SAH. B) SAH grade was calculated by quantifying the blood in the subarachnoidal space by image analysis as described in methods section. (*n* = 6). C) and D) Tail bleeding assay for hemostasis: C) bleeding time and D) blood volume (*n* = 8). (B-D) Student's t-test. Individual values and mean±SEM are shown. (E) CBF in the middle cerebral artery territory was measured by Laser-speckle contrast imager in in *S1pr1*$^{flox/flox}$ and *S1pr1*^{iECKO} mice before (0 min.), 1 min, 10 min, 2 h, 4 h, 24 h after SAH induction. The relative CBF values (%) versus before SAH are shown. Data are mean ± SEM. (*n* = 6). Two-way ANOVA followed by Bonferoni's test showed no statistically significant differences between wild type and *S1PR1*^{iECKO}. Red solid line, *S1PR1*$^{flox/flox}$ ipsilateral side; blue solid, *S1PR1*^{iECKO} ipsilateral; light dotted line, *S1PR1*$^{flox/flox}$ contralateral; light blue dotted line, *S1PR1*^{iECKO} contralateral. IL, ipsilateral side. CL, contralateral side.

Figure 6. Exacerbated cerebral edema and neuronal injury after SAH in endothelial specific S1pr1 null mice A) 72 hours after SAH, brain edema was evaluated by brain water content in *S1pr1*$^{flox/flox}$ and *S1pr1*^{iECKO} mice (*n* = 7 - 14). Brain water content was calculated as ([wet weight-dry weight]/wet weight) x 100. * $p<0.05$, one-way ANOVA followed by Tukey's test. B) Immunofluorescence confocal analysis of phospho-histone H2A.X (DNA damage, green channel). Nuclear staining (DAPI) is shown in the blue channel. Representative images of ipsilateral hemisphere (cortex) from *S1pr1*$^{flox/flox}$ and *S1pr1*^{iECKO} mice after SAH stained are shown. Scale bar,

50 μm. C) Quantification of phospho-histone H2A.X positive cells (%) (n = 7 or 8 mice). *P < 0.05, student's t-test. The individual values and the mean ± SEM are shown. D) Neurological deficits after mild SAH surgery in *S1pr1*$^{flox/flox}$ and *S1pr1*^{iECKO} mice (n = 12 or 14). From 4 to 24 points: 24 points (best), 4 points (worst). Data are mean ± s.e.m. *P < 0.05, **P < 0.01, One-way ANOVA followed by Tukey's test. Red line, *S1pr1*^{iECKO}; Blue line, *S1pr1*$^{flox/flox}$.

Figure 7. Endothelial specific S1pr1 null mice exhibit exacerbated BBB (albumin) leakage after SAH compared to wild type litter-mates. A) Albumin BBB leakage, assessed by Evans Blue Dye extravasation, 24 hours after sham or SAH surgery in *S1pr1*$^{flox/flox}$ and *S1pr1*^{iECKO} mice (n = 6 - 10). Evans blue dye was circulating for 3 hours. The individual values and mean ± SEM are shown. *P < 0.05, **P < 0.01, ***P < 0.001 (One-way ANOVA followed by Tukey's test). y axis shows relative fluorescence units (R.F.U.) per gram of tissue. B) Increased phosphorylation of myosin light chain (p-MLC) in isolated cortical microvessels in *S1pr1*^{iECKO} mice compared to *S1pr1*$^{flox/flox}$. Cortical microvessels were isolated 24 h after SAH in *S1pr1*^{iECKO} and *S1pr1*$^{flox/flox}$ mice. Western blot analysis for phospho-MLC (p-MLC) and β-actin was conducted. Individual values and mean ± SEM are shown. *P < 0.05 (t test).

Table 1. Physiological variables in *S1pr1*$^{flox/flox}$ and *S1pr1*^{iECKO} mice.

Time points	Parameters	*S1pr1*$^{flox/flox}$	*S1pr1*^{iECKO}
5 min before SAH	Arterial O_2 saturation (SpO_2, %)	98.6 ± 0.2	98.4 ± 0.1
	Heart rate (b.p.m.)	442.0 ± 23.2	459.2 ± 10.7
	Pulse distention (μm)	13.8 ± 0.7	12.8 ± 0.9
	Respiratory rate (br.p.m.)	162.3 ± 4.9	155.0 ± 6.7
5 min after SAH	Arterial O_2 saturation (SpO_2, %)	98.6 ± 0.1	98.6 ± 0.2
	Heart rate (b.p.m.)	539.8 ± 9.9	549.7 ± 9.9
	Pulse distention (μm)	13.2 ± 1.1	12.5 ± 0.9
	Respiratory rate (br.p.m.)	133.3 ± 4.4	126.8 ± 6.5

bpm, beats per minute; br.p.m., breaths per minute. Pulse distention is a surrogate for pulse pressure. No significant differences were observed in the physiological parameters (arterial O_2 saturation, heart rate, pulse distention and respiratory rate) between *S1pr1*$^{flox/flox}$ and *S1pr1*^{iECKO} mice, before and after SAH

Table 2. Sequences of the primers used for RT-qPCR	
Target Genes	**Primer's Sequences**
Mouse S1PR1	F: CCGGATCGTATCTTGTTGCA R: AAATTCCATGCCTGGGATGA
Mouse S1PR2	F: ATGGGCGGCTTATACTCAGAG R: GCGCAGCACAAGATGATGAT
Mouse S1PR3	F: GCCTAGCGGGAGAGAAACCT R: CCGACTGCGGGAAGAGTGT
Mouse S1PR4	F: TTAGAGTGGTCCGAGCCAATG R: GATCATCAGCACGGTGTTGAGT
Mouse S1PR5	F: CACCGGCAGTCCTGGAGTA R: AAGGGTTGGGAAGCGTCAGT
18S	F: ACCTCTCGAAGTGTTGGATACAG R: TTCACTAATGACACAAACGTGATTC

REFERENCES

1. Bell RD, Winkler EA, Singh I, Sagare AP, Deane R, Wu Z, Holtzman DM, Betsholtz C, Armulik A, Sallstrom J, Berk BC, Zlokovic BV. Apolipoprotein e controls cerebrovascular integrity via cyclophilin a. *Nature*. 2012;485:512-516
2. Armulik A, Genove G, Mae M, Nisancioglu MH, Wallgard E, Niaudet C, He L, Norlin J, Lindblom P, Strittmatter K, Johansson BR, Betsholtz C. Pericytes regulate the blood-brain barrier. *Nature*. 2010;468:557-561
3. Abbott NJ, Ronnback L, Hansson E. Astrocyte-endothelial interactions at the blood-brain barrier. *Nat Rev Neurosci*. 2006;7:41-53
4. Benjamin EJ, Virani SS, Callaway CW, Chamberlain AM, Chang AR, Cheng S, Chiuve SE, Cushman M, Delling FN, Deo R, de Ferranti SD, Ferguson JF, Fornage M, Gillespie C, Isasi CR, Jimenez MC, Jordan LC, Judd SE, Lackland D, Lichtman JH, Lisabeth L, Liu S, Longenecker CT, Lutsey PL, Mackey JS, Matchar DB, Matsushita K, Mussolino ME, Nasir K, O'Flaherty M, Palaniappan LP, Pandey A, Pandey DK, Reeves MJ, Ritchey MD, Rodriguez CJ, Roth GA, Rosamond WD, Sampson UKA, Satou GM, Shah SH, Spartano NL, Tirschwell DL, Tsao CW, Voeks JH, Willey JZ, Wilkins JT, Wu JH, Alger HM, Wong SS, Muntner P, American Heart Association Council on E, Prevention Statistics C, Stroke Statistics S. Heart disease and stroke statistics-2018 update: A report from the american heart association. *Circulation*. 2018;137:e67-e492
5. Saver JL. Improving reperfusion therapy for acute ischaemic stroke. *J Thromb Haemost*. 2011;9 Suppl 1:333-343
6. Molina CA, Alvarez-Sabin J. Recanalization and reperfusion therapies for acute ischemic stroke. *Cerebrovasc Dis*. 2009;27 Suppl 1:162-167
7. Hamann GF, Okada Y, del Zoppo GJ. Hemorrhagic transformation and microvascular integrity during focal cerebral ischemia/reperfusion. *J Cereb Blood Flow Metab*. 1996;16:1373-1378
8. Ames A, 3rd, Wright RL, Kowada M, Thurston JM, Majno G. Cerebral ischemia. Ii. The no-reflow phenomenon. *Am J Pathol*. 1968;52:437-453
9. del Zoppo GJ, Mabuchi T. Cerebral microvessel responses to focal ischemia. *J Cereb Blood Flow Metab*. 2003;23:879-894
10. Murthy SB, Moradiya Y, Dawson J, Lees KR, Hanley DF, Ziai WC, Butcher K, Davis S, Gregson B, Lyden P, Mayer S, Muir K, Steiner T. Perihematomal edema and functional outcomes in intracerebral hemorrhage. *Influence of Hematoma Volume and Location*. 2015;46:3088-3092
11. Macdonald RL, Pluta RM, Zhang JH. Cerebral vasospasm after subarachnoid hemorrhage: The emerging revolution. *Nature clinical practice. Neurology*. 2007;3:256-263
12. Macdonald RL. Delayed neurological deterioration after subarachnoid haemorrhage. *Nat Rev Neurol*. 2014;10:44-58
13. Pluta RM, Hansen-Schwartz J, Dreier J, Vajkoczy P, Macdonald RL, Nishizawa S, Kasuya H, Wellman G, Keller E, Zauner A, Dorsch N, Clark J, Ono S, Kiris T, Leroux P, Zhang JH. Cerebral vasospasm following subarachnoid hemorrhage: Time for a new world of thought. *Neurol Res*. 2009;31:151-158
14. Venkataraman K, Lee YM, Michaud J, Thangada S, Ai Y, Bonkovsky HL, Parikh NS, Habrukowich C, Hla T. Vascular endothelium as a contributor of plasma sphingosine 1-phosphate. *Circ Res*. 2008;102:669-676
15. Fukuhara S, Simmons S, Kawamura S, Inoue A, Orba Y, Tokudome T, Sunden Y, Arai Y, Moriwaki K, Ishida J, Uemura A, Kiyonari H, Abe T, Fukamizu A, Hirashima M, Sawa H, Aoki J, Ishii M, Mochizuki N. The sphingosine-1-phosphate transporter spns2 expressed on endothelial cells regulates lymphocyte trafficking in mice. *J Clin Invest*. 2012;122:1416-1426
16. Pappu R, Schwab SR, Cornelissen I, Pereira JP, Regard JB, Xu Y, Camerer E, Zheng YW, Huang Y, Cyster JG, Coughlin SR. Promotion of lymphocyte egress into blood and lymph by distinct sources of sphingosine-1-phosphate. *Science*. 2007;316:295-298

17. Murata N, Sato K, Kon J, Tomura H, Yanagita M, Kuwabara A, Ui M, Okajima F. Interaction of sphingosine 1-phosphate with plasma components, including lipoproteins, regulates the lipid receptor-mediated actions. *Biochem J*. 2000;352 Pt 3:809-815
18. Christoffersen C, Obinata H, Kumaraswamy SB, Galvani S, Ahnstrom J, Sevvana M, Egerer-Sieber C, Muller YA, Hla T, Nielsen LB, Dahlback B. Endothelium-protective sphingosine-1-phosphate provided by hdl-associated apolipoprotein m. *Proc Natl Acad Sci U S A*. 2011;108:9613-9618
19. Liu Y, Wada R, Yamashita T, Mi Y, Deng CX, Hobson JP, Rosenfeldt HM, Nava VE, Chae SS, Lee MJ, Liu CH, Hla T, Spiegel S, Proia RL. Edg-1, the g protein-coupled receptor for sphingosine-1-phosphate, is essential for vascular maturation. *J Clin Invest*. 2000;106:951-961
20. Allende ML, Yamashita T, Proia RL. G-protein-coupled receptor s1p1 acts within endothelial cells to regulate vascular maturation. *Blood*. 2003;102:3665-3667
21. Jung B, Obinata H, Galvani S, Mendelson K, Ding BS, Skoura A, Kinzel B, Brinkmann V, Rafii S, Evans T, Hla T. Flow-regulated endothelial s1p receptor-1 signaling sustains vascular development. *Developmental cell*. 2012;23:600-610
22. Lee MJ, Thangada S, Claffey KP, Ancellin N, Liu CH, Kluk M, Volpi M, Sha'afi RI, Hla T. Vascular endothelial cell adherens junction assembly and morphogenesis induced by sphingosine-1-phosphate. *Cell*. 1999;99:301-312
23. Sanchez T, Estrada-Hernandez T, Paik JH, Wu MT, Venkataraman K, Brinkmann V, Claffey K, Hla T. Phosphorylation and action of the immunomodulator fty720 inhibits vascular endothelial cell growth factor-induced vascular permeability. *J Biol Chem*. 2003;278:47281-47290
24. Galvani S, Sanson M, Blaho VA, Swendeman SL, Conger H, Dahlback B, Kono M, Proia RL, Smith JD, Hla T. Hdl-bound sphingosine 1-phosphate acts as a biased agonist for the endothelial cell receptor s1p1 to limit vascular inflammation. *Science signaling*. 2015;8:ra79
25. Sanchez T. Sphingosine-1-phosphate signaling in endothelial disorders. *Current atherosclerosis reports*. 2016;18:31
26. Kimura T, Sato K, Kuwabara A, Tomura H, Ishiwara M, Kobayashi I, Ui M, Okajima F. Sphingosine 1-phosphate may be a major component of plasma lipoproteins responsible for the cytoprotective actions in human umbilical vein endothelial cells. *J Biol Chem*. 2001;276:31780-31785
27. Wilkerson BA, Grass GD, Wing SB, Argraves WS, Argraves KM. Sphingosine 1-phosphate (s1p) carrier-dependent regulation of endothelial barrier: High density lipoprotein (hdl)-s1p prolongs endothelial barrier enhancement as compared with albumin-s1p via effects on levels, trafficking, and signaling of s1p1. *J Biol Chem*. 2012;287:44645-44653
28. Sattler K, Graler M, Keul P, Weske S, Reimann CM, Jindrova H, Kleinbongard P, Sabbadini R, Brocker-Preuss M, Erbel R, Heusch G, Levkau B. Defects of high-density lipoproteins in coronary artery disease caused by low sphingosine-1-phosphate content: Correction by sphingosine-1-phosphate-loading. *Journal of the American College of Cardiology*. 2015;66:1470-1485
29. Sattler K, Lehmann I, Graler M, Brocker-Preuss M, Erbel R, Heusch G, Levkau B. Hdl-bound sphingosine 1-phosphate (s1p) predicts the severity of coronary artery atherosclerosis. *Cellular physiology and biochemistry : international journal of experimental cellular physiology, biochemistry, and pharmacology*. 2014;34:172-184
30. Frej C, Linder A, Happonen KE, Taylor FB, Lupu F, Dahlback B. Sphingosine 1-phosphate and its carrier apolipoprotein m in human sepsis and in escherichia coli sepsis in baboons. *Journal of cellular and molecular medicine*. 2016;20:1170-1181
31. Plomgaard P, Dullaart RP, de Vries R, Groen AK, Dahlback B, Nielsen LB. Apolipoprotein m predicts pre-beta-hdl formation: Studies in type 2 diabetic and nondiabetic subjects. *Journal of internal medicine*. 2009;266:258-267
32. Ruiz M, Frej C, Holmer A, Guo LJ, Tran S, Dahlback B. High-density lipoprotein-associated apolipoprotein m limits endothelial inflammation by delivering sphingosine-1-phosphate to the sphingosine-1-phosphate receptor 1. *Arterioscler Thromb Vasc Biol*. 2017;37:118-129

33. Frej C, Mendez AJ, Ruiz M, Castillo M, Hughes TA, Dahlback B, Goldberg RB. A shift in apom/s1p between hdl-particles in women with type 1 diabetes mellitus is associated with impaired anti-inflammatory effects of the apom/s1p complex. *Arterioscler Thromb Vasc Biol*. 2017;37:1194-1205
34. Matloubian M, Lo CG, Cinamon G, Lesneski MJ, Xu Y, Brinkmann V, Allende ML, Proia RL, Cyster JG. Lymphocyte egress from thymus and peripheral lymphoid organs is dependent on s1p receptor 1. *Nature*. 2004;427:355-360
35. Brinkmann V, Davis MD, Heise CE, Albert R, Cottens S, Hof R, Bruns C, Prieschl E, Baumruker T, Hiestand P, Foster CA, Zollinger M, Lynch KR. The immune modulator fty720 targets sphingosine 1-phosphate receptors. *J Biol Chem*. 2002;277:21453-21457.
36. Brinkmann V, Billich A, Baumruker T, Heining P, Schmouder R, Francis G, Aradhye S, Burtin P. Fingolimod (fty720): Discovery and development of an oral drug to treat multiple sclerosis. *Nat Rev Drug Discov*. 2010;9:883-897
37. LaMontagne K, Littlewood-Evans A, Schnell C, O'Reilly T, Wyder L, Sanchez T, Probst B, Butler J, Wood A, Liau G, Billy E, Theuer A, Hla T, Wood J. Antagonism of sphingosine-1-phosphate receptors by fty720 inhibits angiogenesis and tumor vascularization. *Cancer Res*. 2006;66:221-231
38. Oo ML, Chang SH, Thangada S, Wu MT, Rezaul K, Blaho V, Hwang SI, Han DK, Hla T. Engagement of s1p(1)-degradative mechanisms leads to vascular leak in mice. *J Clin Invest*. 2011;121:2290-2300
39. Hasegawa Y, Suzuki H, Sozen T, Rolland W, Zhang JH. Activation of sphingosine 1-phosphate receptor-1 by fty720 is neuroprotective after ischemic stroke in rats. *Stroke*. 2010;41:368-374
40. Wei Y, Yemisci M, Kim HH, Yung LM, Shin HK, Hwang SK, Guo S, Qin T, Alsharif N, Brinkmann V, Liao JK, Lo EH, Waeber C. Fingolimod provides long-term protection in rodent models of cerebral ischemia. *Ann Neurol*. 2011
41. Brait VH, Tarrason G, Gavalda A, Godessart N, Planas AM. Selective sphingosine 1-phosphate receptor 1 agonist is protective against ischemia/reperfusion in mice. *Stroke*. 2016;47:3053-3056
42. Kraft P, Gob E, Schuhmann MK, Gobel K, Deppermann C, Thielmann I, Herrmann AM, Lorenz K, Brede M, Stoll G, Meuth SG, Nieswandt B, Pfeilschifter W, Kleinschnitz C. Fty720 ameliorates acute ischemic stroke in mice by reducing thrombo-inflammation but not by direct neuroprotection. *Stroke*. 2013;44:3202-3210
43. Vogelgesang A, Grunwald U, Langner S, Jack R, Broker BM, Kessler C, Dressel A. Analysis of lymphocyte subsets in patients with stroke and their influence on infection after stroke. *Stroke*. 2008;39:237-241
44. Dirnagl U, Klehmet J, Braun JS, Harms H, Meisel C, Ziemssen T, Prass K, Meisel A. Stroke-induced immunodepression: Experimental evidence and clinical relevance. *Stroke*. 2007;38:770-773
45. Yanagida K, Liu CH, Faraco G, Galvani S, Smith HK, Burg N, Anrather J, Sanchez T, Iadecola C, Hla T. Size-selective opening of the blood-brain barrier by targeting endothelial sphingosine 1-phosphate receptor 1. *Proc Natl Acad Sci U S A*. 2017;114:4531–4536
46. Pitulescu ME, Schmidt I, Benedito R, Adams RH. Inducible gene targeting in the neonatal vasculature and analysis of retinal angiogenesis in mice. *Nature protocols*. 2010;5:1518-1534
47. Cahalan SM, Gonzalez-Cabrera PJ, Sarkisyan G, Nguyen N, Schaeffer MT, Huang L, Yeager A, Clemons B, Scott F, Rosen H. Actions of a picomolar short-acting s1p(1) agonist in s1p(1)-egfp knock-in mice. *Nat Chem Biol*. 2011;7:254-256
48. Kamii H, Tominaga T. Filament perforation subarachnoid hemorrhage: Mouse model. *Animal Models of Acute Neurological Injuries (Chen J, Xu X-M, Xu ZC, Zhang JH, editors). Humana Press, Totowa, NJ*. 2009;Chapter 23:279-286
49. Kluk MJ, Ryan KP, Wang B, Zhang G, Rodig SJ, Sanchez T. Sphingosine-1-phosphate receptor 1 in classical hodgkin lymphoma: Assessment of expression and role in cell migration. *Lab Invest*. 2013;93:462-471

50. Lee Y, Uchida H, Smith H, Ito A, Sanchez T. The isolation and molecular characterization of cerebral microvessels. . *Nature protocols*. 2019 (In press)
51. Sugawara T, Ayer R, Jadhav V, Zhang JH. A new grading system evaluating bleeding scale in filament perforation subarachnoid hemorrhage rat model. *Journal of neuroscience methods*. 2008;167:327-334
52. Liu Y, Jennings NL, Dart AM, Du XJ. Standardizing a simpler, more sensitive and accurate tail bleeding assay in mice. *World journal of experimental medicine*. 2012;2:30-36
53. Parra A, McGirt MJ, Sheng H, Laskowitz DT, Pearlstein RD, Warner DS. Mouse model of subarachnoid hemorrhage associated cerebral vasospasm: Methodological analysis. *Neurol Res*. 2002;24:510-516
54. Vellimana AK, Milner E, Azad TD, Harries MD, Zhou ML, Gidday JM, Han BH, Zipfel GJ. Endothelial nitric oxide synthase mediates endogenous protection against subarachnoid hemorrhage-induced cerebral vasospasm. *Stroke*. 2011;42:776-782
55. Adachi M, Feigin I. Cerebral oedema and the water content of normal white matter. *Journal of neurology, neurosurgery, and psychiatry*. 1966;29:446-450
56. Lu C, Zhu F, Cho YY, Tang F, Zykova T, Ma WY, Bode AM, Dong Z. Cell apoptosis: Requirement of h2ax in DNA ladder formation, but not for the activation of caspase-3. *Mol Cell*. 2006;23:121-132
57. Sharma A, Singh K, Almasan A. Histone h2ax phosphorylation: A marker for DNA damage. *Methods Mol Biol*. 2012;920:613-626
58. Shi Y, Zhang L, Pu H, Mao L, Hu X, Jiang X, Xu N, Stetler RA, Zhang F, Liu X, Leak RK, Keep RF, Ji X, Chen J. Rapid endothelial cytoskeletal reorganization enables early blood–brain barrier disruption and long-term ischaemic reperfusion brain injury. *Nature communications*. 2016;7:10523
59. Uyama O, Okamura N, Yanase M, Narita M, Kawabata K, Sugita M. Quantitative evaluation of vascular permeability in the gerbil brain after transient ischemia using evans blue fluorescence. *J Cereb Blood Flow Metab*. 1988;8:282-284
60. Zhang G, Yang L, Kim GS, Ryan K, Lu S, O'Donnell RK, Spokes K, Shapiro N, Aird WC, Kluk MJ, Yano K, Sanchez T. Critical role of sphingosine-1-phosphate receptor 2 (s1pr2) in acute vascular inflammation. *Blood*. 2013;122:443-455
61. Shih SC, Smith LE. Quantitative multi-gene transcriptional profiling using real-time pcr with a master template. *Exp Mol Pathol*. 2005;79:14-22
62. Montesano R, Pepper MS, Mohle-Steinlein U, Risau W, Wagner EF, Orci L. Increased proteolytic activity is responsible for the aberrant morphogenetic behavior of endothelial cells expressing the middle t oncogene. *Cell*. 1990;62:435-445
63. Muroi C, Fujioka M, Marbacher S, Fandino J, Keller E, Iwasaki K, Mishima K. Mouse model of subarachnoid hemorrhage: Technical note on the filament perforation model. *Acta Neurochir Suppl*. 2015;120:315-320
64. Knowland D, Arac A, Sekiguchi KJ, Hsu M, Lutz SE, Perrino J, Steinberg GK, Barres BA, Nimmerjahn A, Agalliu D. Stepwise recruitment of transcellular and paracellular pathways underlies blood-brain barrier breakdown in stroke. *Neuron*. 2014;82:603-617
65. Rosenberg GA, Yang Y. Vasogenic edema due to tight junction disruption by matrix metalloproteinases in cerebral ischemia. *Neurosurgical focus*. 2007;22:E4
66. Yang Y, Estrada EY, Thompson JF, Liu W, Rosenberg GA. Matrix metalloproteinase-mediated disruption of tight junction proteins in cerebral vessels is reversed by synthetic matrix metalloproteinase inhibitor in focal ischemia in rat. *J Cereb Blood Flow Metab*. 2007;27:697-709
67. Nitta T, Hata M, Gotoh S, Seo Y, Sasaki H, Hashimoto N, Furuse M, Tsukita S. Size-selective loosening of the blood-brain barrier in claudin-5-deficient mice. *J Cell Biol*. 2003;161:653-660
68. Kuhlmann CR, Tamaki R, Gamerdinger M, Lessmann V, Behl C, Kempski OS, Luhmann HJ. Inhibition of the myosin light chain kinase prevents hypoxia-induced blood-brain barrier disruption. *J Neurochem*. 2007;102:501-507

69. Vandenbroucke E, Mehta D, Minshall R, Malik AB. Regulation of endothelial junctional permeability. *Ann N Y Acad Sci*. 2008;1123:134-145
70. Sadeghian H, Lacoste B, Qin T, Toussay X, Rosa R, Oka F, Chung DY, Takizawa T, Gu C, Ayata C. Spreading depolarizations trigger caveolin-1–dependent endothelial transcytosis. *Annals of Neurology*. 2018;84:409-423
71. Shlosberg D, Benifla M, Kaufer D, Friedman A. Blood-brain barrier breakdown as a therapeutic target in traumatic brain injury. *Nat Rev Neurol*. 2010;6:393-403
72. Chodobski A, Zink BJ, Szmydynger-Chodobska J. Blood-brain barrier pathophysiology in traumatic brain injury. *Translational stroke research*. 2011;2:492-516
73. Kenney K, Amyot F, Haber M, Pronger A, Bogoslovsky T, Moore C, Diaz-Arrastia R. Cerebral vascular injury in traumatic brain injury. *Experimental Neurology*. 2016;275:353-366
74. Pitkanen A, Loscher W, Vezzani A, Becker AJ, Simonato M, Lukasiuk K, Grohn O, Bankstahl JP, Friedman A, Aronica E, Gorter JA, Ravizza T, Sisodiya SM, Kokaia M, Beck H. Advances in the development of biomarkers for epilepsy. *Lancet Neurol*. 2016;15:843-856
75. Iacobone E, Bailly-Salin J, Polito A, Friedman D, Stevens RD, Sharshar T. Sepsis-associated encephalopathy and its differential diagnosis. *Critical care medicine*. 2009;37:S331-336
76. Nation DA, Sweeney MD, Montagne A, Sagare AP, D'Orazio LM, Pachicano M, Sepehrband F, Nelson AR, Buennagel DP, Harrington MG, Benzinger TLS, Fagan AM, Ringman JM, Schneider LS, Morris JC, Chui HC, Law M, Toga AW, Zlokovic BV. Blood-brain barrier breakdown is an early biomarker of human cognitive dysfunction. *Nat Med*. 2019
77. Montagne A, Barnes SR, Sweeney MD, Halliday MR, Sagare AP, Zhao Z, Toga AW, Jacobs RE, Liu CY, Amezcua L, Harrington MG, Chui HC, Law M, Zlokovic BV. Blood-brain barrier breakdown in the aging human hippocampus. *Neuron*. 2015;85:296-302
78. Zlokovic BV. The blood-brain barrier in health and chronic neurodegenerative disorders. *Neuron*. 2008;57:178-201
79. Doherty CP, O'Keefe E, Wallace E, Loftus T, Keaney J, Kealy J, Humphries MM, Molloy MG, Meaney JF, Farrell M, Campbell M. Blood-brain barrier dysfunction as a hallmark pathology in chronic traumatic encephalopathy. *J Neuropathol Exp Neurol*. 2016;75:656-662
80. Faraci FM. Vascular protection. *Stroke*. 2003;34:327-329
81. Aird WC. Spatial and temporal dynamics of the endothelium. *J Thromb Haemost*. 2005;3:1392-1406
82. Johnston SC, Selvin S, Gress DR. The burden, trends, and demographics of mortality from subarachnoid hemorrhage. *Neurology*. 1998;50:1413-1418
83. van Gijn J, Kerr RS, Rinkel GJ. Subarachnoid haemorrhage. *Lancet*. 2007;369:306-318
84. Al-Khindi T, Macdonald RL, Schweizer TA. Cognitive and functional outcome after aneurysmal subarachnoid hemorrhage. *Stroke*. 2010;41:e519-536
85. Dóczi T. The pathogenetic and prognostic significance of blood-brain barrier damage at the acute stage of aneurysmal subarachnoid haemorrhage. Clinical and experimental studies. *Acta Neurochirurgica*. 1985;77:110-132
86. Park S, Yamaguchi M, Zhou C, Calvert JW, Tang J, Zhang JH. Neurovascular protection reduces early brain injury after subarachnoid hemorrhage. *Stroke*. 2004;35:2412-2417
87. Lackner P, Dietmann A, Beer R, Fischer M, Broessner G, Helbok R, Marxgut J, Pfausler B, Schmutzhard E. Cellular microparticles as a marker for cerebral vasospasm in spontaneous subarachnoid hemorrhage. *Stroke*. 2010;41:2353-2357
88. Fischer M, Broessner G, Dietmann A, Beer R, Helbok R, Pfausler B, Chemelli A, Schmutzhard E, Lackner P. Angiopoietin-1 is associated with cerebral vasospasm and delayed cerebral ischemia in subarachnoid hemorrhage. *BMC neurology*. 2011;11:59
89. Suzuki H, Hasegawa Y, Kanamaru K, Zhang JH. Mechanisms of osteopontin-induced stabilization of blood-brain barrier disruption after subarachnoid hemorrhage in rats. *Stroke*. 2010;41:1783-1790

90. Altay O, Suzuki H, Hasegawa Y, Caner B, Krafft PR, Fujii M, Tang J, Zhang JH. Isoflurane attenuates blood-brain barrier disruption in ipsilateral hemisphere after subarachnoid hemorrhage in mice. *Stroke*. 2012;43:2513-2516
91. Wang Z, Meng CJ, Shen XM, Shu Z, Ma C, Zhu GQ, Liu HX, He WC, Sun XB, Huo L, Zhang J, Chen G. Potential contribution of hypoxia-inducible factor-1alpha, aquaporin-4, and matrix metalloproteinase-9 to blood-brain barrier disruption and brain edema after experimental subarachnoid hemorrhage. *Journal of molecular neuroscience : MN*. 2012;48:273-280
92. Egashira Y, Zhao H, Hua Y, Keep RF, Xi G. White matter injury after subarachnoid hemorrhage: Role of blood-brain barrier disruption and matrix metalloproteinase-9. *Stroke*. 2015;46:2909-2915
93. Sehba FA, Mostafa G, Knopman J, Friedrich V, Jr., Bederson JB. Acute alterations in microvascular basal lamina after subarachnoid hemorrhage. *J Neurosurg*. 2004;101:633-640
94. Siler DA, Berlow YA, Kukino A, Davis CM, Nelson JW, Grafe MR, Ono H, Cetas JS, Pike M, Alkayed NJ. Soluble epoxide hydrolase in hydrocephalus, cerebral edema, and vascular inflammation after subarachnoid hemorrhage. *Stroke*. 2015;46:1916-1922
95. Pan S, Gray NS, Gao W, Mi Y, Fan Y, Wang X, Tuntland T, Che J, Lefebvre S, Chen Y, Chu A, Hinterding K, Gardin A, End P, Heining P, Bruns C, Cooke NG, Nuesslein-Hildesheim B. Discovery of baf312 (siponimod), a potent and selective s1p receptor modulator. *ACS medicinal chemistry letters*. 2013;4:333-337
96. Gergely P, Nuesslein-Hildesheim B, Guerini D, Brinkmann V, Traebert M, Bruns C, Pan S, Gray NS, Hinterding K, Cooke NG, Groenewegen A, Vitaliti A, Sing T, Luttringer O, Yang J, Gardin A, Wang N, Crumb WJ, Jr., Saltzman M, Rosenberg M, Wallstrom E. The selective sphingosine 1-phosphate receptor modulator baf312 redirects lymphocyte distribution and has species-specific effects on heart rate. *Br J Pharmacol*. 2012;167:1035-1047
97. Quancard J, Bollbuck B, Janser P, Angst D, Berst F, Buehlmayer P, Streiff M, Beerli C, Brinkmann V, Guerini D, Smith Paul A, Seabrook Timothy J, Traebert M, Seuwen K, Hersperger R, Bruns C, Bassilana F, Bigaud M. A potent and selective s1p1 antagonist with efficacy in experimental autoimmune encephalomyelitis. *Chemistry & Biology*. 2012;19:1142-1151
98. Fu Y, Hao J, Zhang N, Ren L, Sun N, Li YJ, Yan Y, Huang D, Yu C, Shi FD. Fingolimod for the treatment of intracerebral hemorrhage: A 2-arm proof-of-concept study. *JAMA neurology*. 2014;71:1092-1101
99. Fu Y, Zhang N, Ren L, Yan Y, Sun N, Li YJ, Han W, Xue R, Liu Q, Hao J, Yu C, Shi FD. Impact of an immune modulator fingolimod on acute ischemic stroke. *Proc Natl Acad Sci U S A*. 2014;111:18315-18320
100. Zhu Z, Fu Y, Tian D, Sun N, Han W, Chang G, Dong Y, Xu X, Liu Q, Huang D, Shi FD. Combination of an immune modulator fingolimod with alteplase in acute ischemic stroke: A pilot trial. *Circulation*. 2015
101. Weissberg I, Wood L, Kamintsky L, Vazquez O, Milikovsky DZ, Alexander A, Oppenheim H, Ardizzone C, Becker A, Frigerio F, Vezzani A, Buckwalter MS, Huguenard JR, Friedman A, Kaufer D. Albumin induces excitatory synaptogenesis through astrocytic tgf-beta/alk5 signaling in a model of acquired epilepsy following blood-brain barrier dysfunction. *Neurobiol Dis*. 2015;78:115-125
102. Petersen MA, Ryu JK, Akassoglou K. Fibrinogen in neurological diseases: Mechanisms, imaging and therapeutics. *Nat Rev Neurosci*. 2018;19:283-301
103. Keep RF, Andjelkovic AV, Xiang J, Stamatovic SM, Antonetti DA, Hua Y, Xi G. Brain endothelial cell junctions after cerebral hemorrhage: Changes, mechanisms and therapeutic targets. *J Cereb Blood Flow Metab*. 2018:271678X18774666
104. Obermeier B, Daneman R, Ransohoff RM. Development, maintenance and disruption of the blood-brain barrier. *Nat Med*. 2013;19:1584-1596
105. Liebner S, Dijkhuizen RM, Reiss Y, Plate KH, Agalliu D, Constantin G. Functional morphology of the blood–brain barrier in health and disease. *Acta Neuropathologica*. 2018;135:311-336

106. Nag S. Morphology and molecular properties of cellular components of normal cerebral vessels. *Methods in molecular medicine*. 2003;89:3-36
107. Daneman R, Zhou L, Kebede AA, Barres BA. Pericytes are required for blood-brain barrier integrity during embryogenesis. *Nature*. 2010;468:562-566
108. Gasche Y, Fujimura M, Morita-Fujimura Y, Copin JC, Kawase M, Massengale J, Chan PH. Early appearance of activated matrix metalloproteinase-9 after focal cerebral ischemia in mice: A possible role in blood-brain barrier dysfunction. *J Cereb Blood Flow Metab*. 1999;19:1020-1028
109. Rosenberg GA, Estrada EY, Dencoff JE. Matrix metalloproteinases and timps are associated with blood-brain barrier opening after reperfusion in rat brain. *Stroke*. 1998;29:2189-2195
110. Asahi M, Sumii T, Fini ME, Itohara S, Lo EH. Matrix metalloproteinase 2 gene knockout has no effect on acute brain injury after focal ischemia. *Neuroreport*. 2001;12:3003-3007
111. Asahi M, Wang X, Mori T, Sumii T, Jung JC, Moskowitz MA, Fini ME, Lo EH. Effects of matrix metalloproteinase-9 gene knock-out on the proteolysis of blood-brain barrier and white matter components after cerebral ischemia. *J Neurosci*. 2001;21:7724-7732
112. Hamann GF, Okada Y, Fitridge R, del Zoppo GJ. Microvascular basal lamina antigens disappear during cerebral ischemia and reperfusion. *Stroke*. 1995;26:2120-2126
113. Günzel D, Yu ASL. Claudins and the modulation of tight junction permeability. *Physiological reviews*. 2013;93:525-569
114. Kondo T, Reaume AG, Huang TT, Carlson E, Murakami K, Chen SF, Hoffman EK, Scott RW, Epstein CJ, Chan PH. Reduction of cuzn-superoxide dismutase activity exacerbates neuronal cell injury and edema formation after transient focal cerebral ischemia. *J Neurosci*. 1997;17:4180-4189
115. Asahi M, Asahi K, Jung JC, del Zoppo GJ, Fini ME, Lo EH. Role for matrix metalloproteinase 9 after focal cerebral ischemia: Effects of gene knockout and enzyme inhibition with bb-94. *J Cereb Blood Flow Metab*. 2000;20:1681-1689
116. Dvorak HF. Vascular permeability to plasma, plasma proteins, and cells: An update. *Curr Opin Hematol*. 2010;17:225-229
117. Reeson P, Tennant KA, Gerrow K, Wang J, Weiser Novak S, Thompson K, Lockhart K-L, Holmes A, Nahirney PC, Brown CE. Delayed inhibition of vegf signaling after stroke attenuates blood–brain barrier breakdown and improves functional recovery in a comorbidity-dependent manner. *The Journal of Neuroscience*. 2015;35:5128-5143
118. Gurnik S, Devraj K, Macas J, Yamaji M, Starke J, Scholz A, Sommer K, Di Tacchio M, Vutukuri R, Beck H, Mittelbronn M, Foerch C, Pfeilschifter W, Liebner S, Peters KG, Plate KH, Reiss Y. Angiopoietin-2-induced blood–brain barrier compromise and increased stroke size are rescued by ve-ptp-dependent restoration of tie2 signaling. *Acta Neuropathologica*. 2016;131:753-773
119. Kappos L, Li DK, Stuve O, Hartung HP, Freedman MS, Hemmer B, Rieckmann P, Montalban X, Ziemssen T, Hunter B, Arnould S, Wallstrom E, Selmaj K. Safety and efficacy of siponimod (baf312) in patients with relapsing-remitting multiple sclerosis: Dose-blinded, randomized extension of the phase 2 bold study. *JAMA neurology*. 2016;73:1089-1098
120. Kappos L, Radue EW, O'Connor P, Polman C, Hohlfeld R, Calabresi P, Selmaj K, Agoropoulou C, Leyk M, Zhang-Auberson L, Burtin P, Group FS. A placebo-controlled trial of oral fingolimod in relapsing multiple sclerosis. *N Engl J Med*. 2010;362:387-401
121. Cohen JA, Barkhof F, Comi G, Hartung HP, Khatri BO, Montalban X, Pelletier J, Capra R, Gallo P, Izquierdo G, Tiel-Wilck K, de Vera A, Jin J, Stites T, Wu S, Aradhye S, Kappos L, Group TS. Oral fingolimod or intramuscular interferon for relapsing multiple sclerosis. *N Engl J Med*. 2010;362:402-415
122. Linda H, von Heijne A. A case of posterior reversible encephalopathy syndrome associated with gilenya((r)) (fingolimod) treatment for multiple sclerosis. *Frontiers in neurology*. 2015;6:39

123. Kim GS, Yang L, Zhang G, Zhao H, Selim M, McCullough LD, Kluk MJ, Sanchez T. Critical role of sphingosine-1-phosphate receptor-2 in the disruption of cerebrovascular integrity in experimental stroke. *Nature communications*. 2015;6:7893
124. Swendeman SL, Xiong Y, Cantalupo A, Yuan H, Burg N, Hisano Y, Cartier A, Liu CH, Engelbrecht E, Blaho V, Zhang Y, Yanagida K, Galvani S, Obinata H, Salmon JE, Sanchez T, Di Lorenzo A, Hla T. An engineered s1p chaperone attenuates hypertension and ischemic injury. *Science signaling*. 2017;10

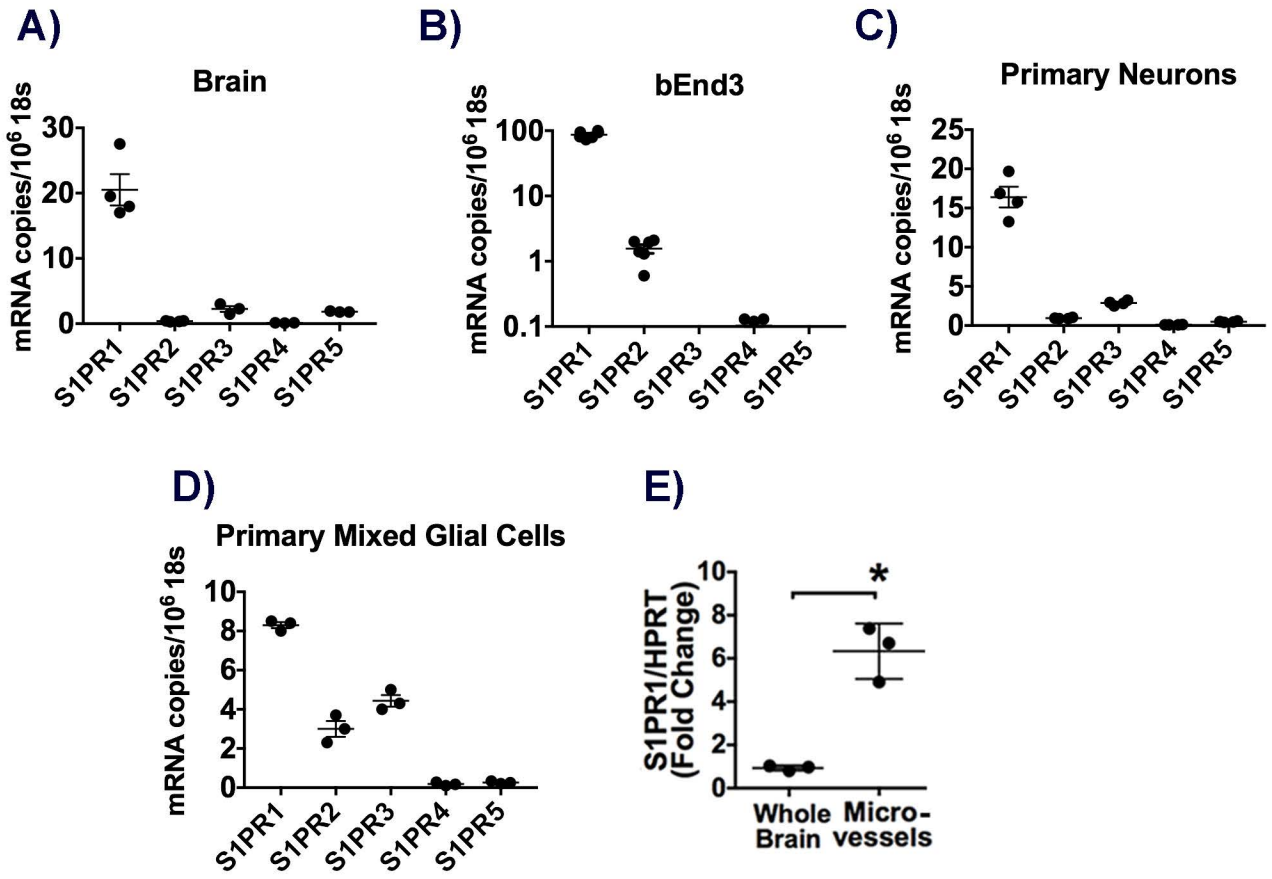
A)
Brain
mRNA copies/10^6 18s
30
20
10
0
S1PR1
S1PR2
S1PR3
S1PR4
S1PR5
B)
bEnd3
mRNA copies/10^6 18s
100
10
1
0.1
S1PR1
S1PR2
S1PR3
S1PR4
S1PR5
C)
Primary Neurons
mRNA copies/10^6 18s
25
20
15
10
5
0
S1PR1
S1PR2
S1PR3
S1PR4
S1PR5
D)
Primary Mixed Glial Cells
mRNA copies/10^6 18s
10
8
6
4
2
0
S1PR1
S1PR2
S1PR3
S1PR4
S1PR5
E)
S1PR1/HPRT
(Fold Change)
10
8
6
4
2
0
*
Whole
Brain
Micro-
vessels

Figure 1

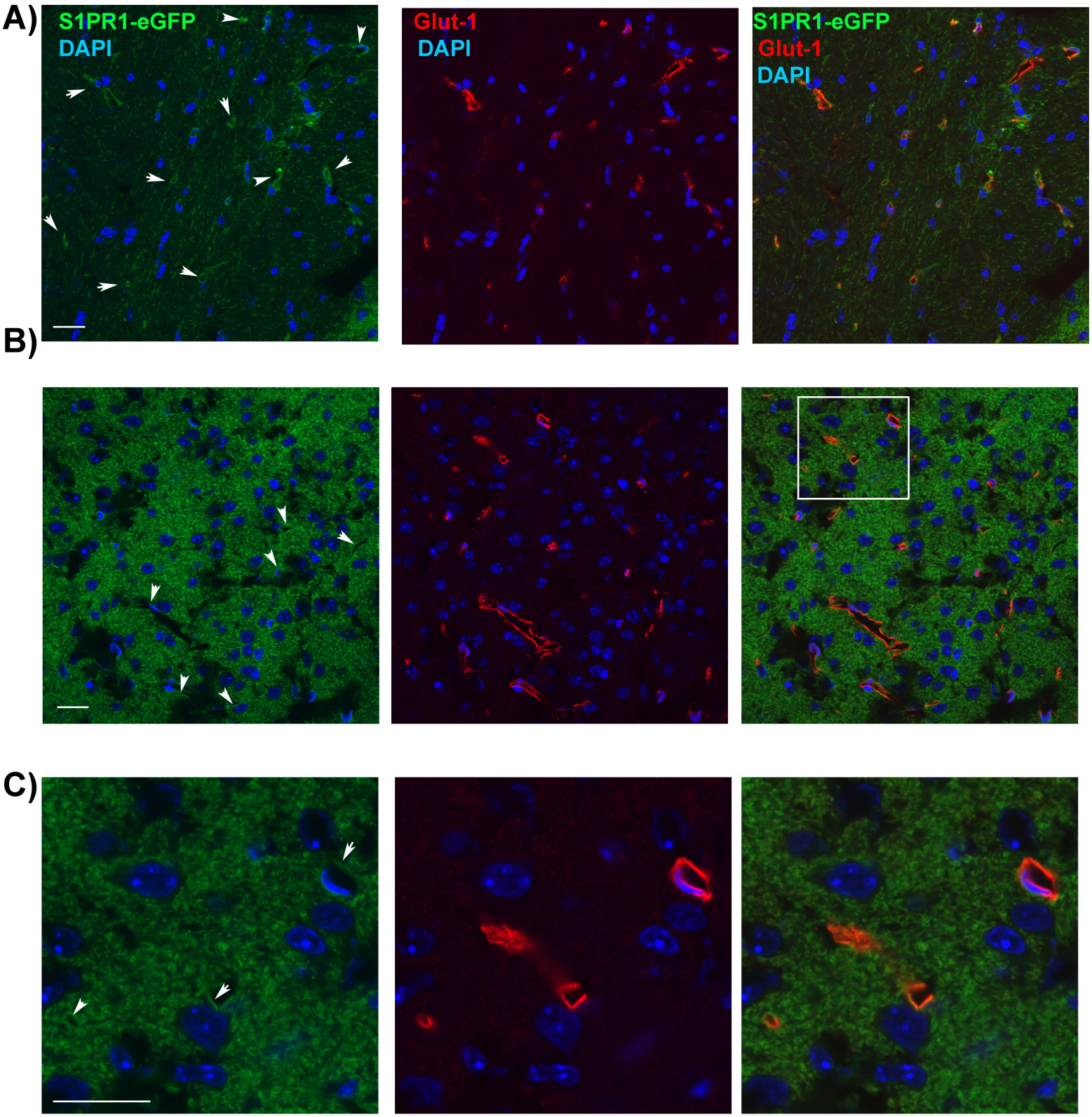

Figure 2

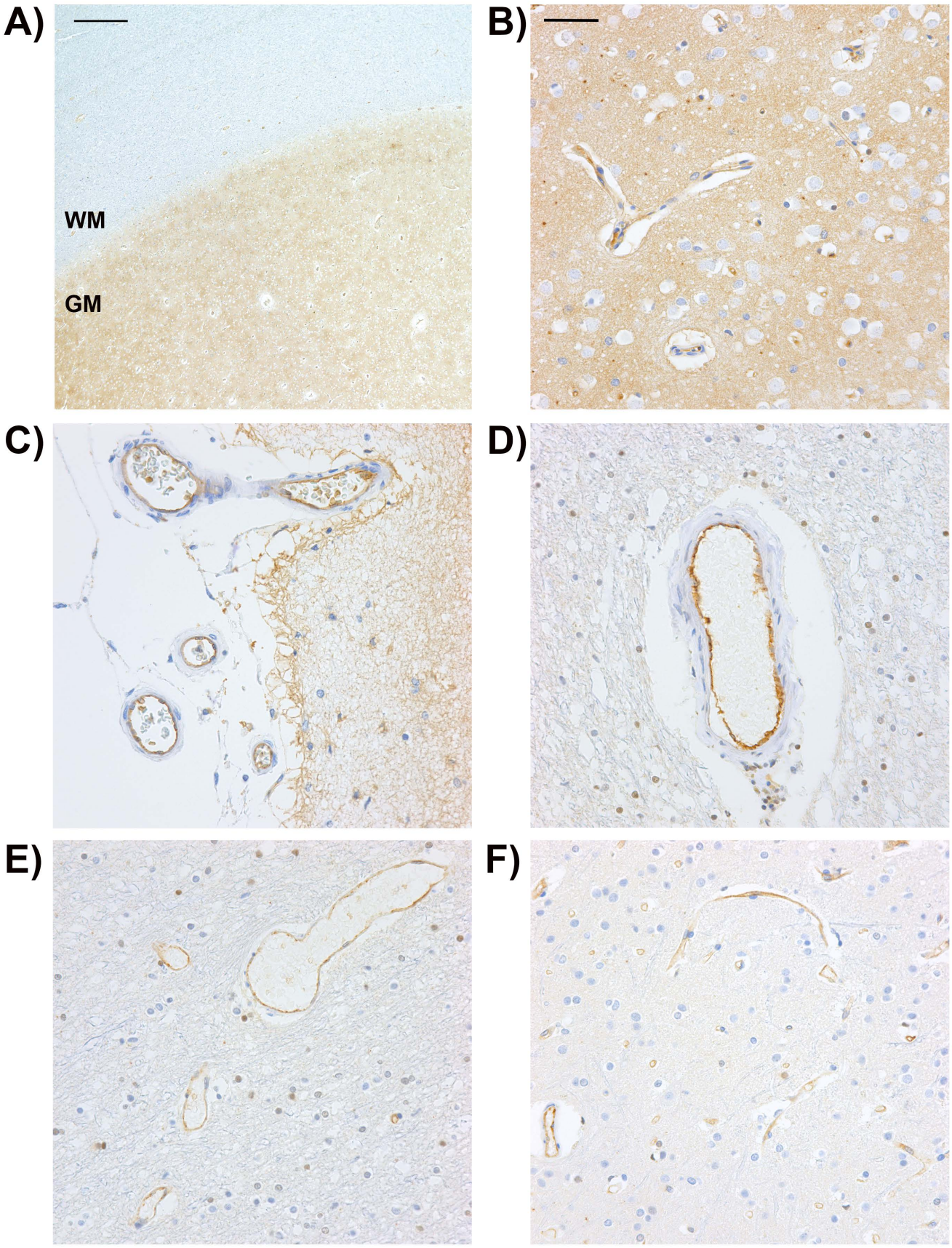

Figure 3

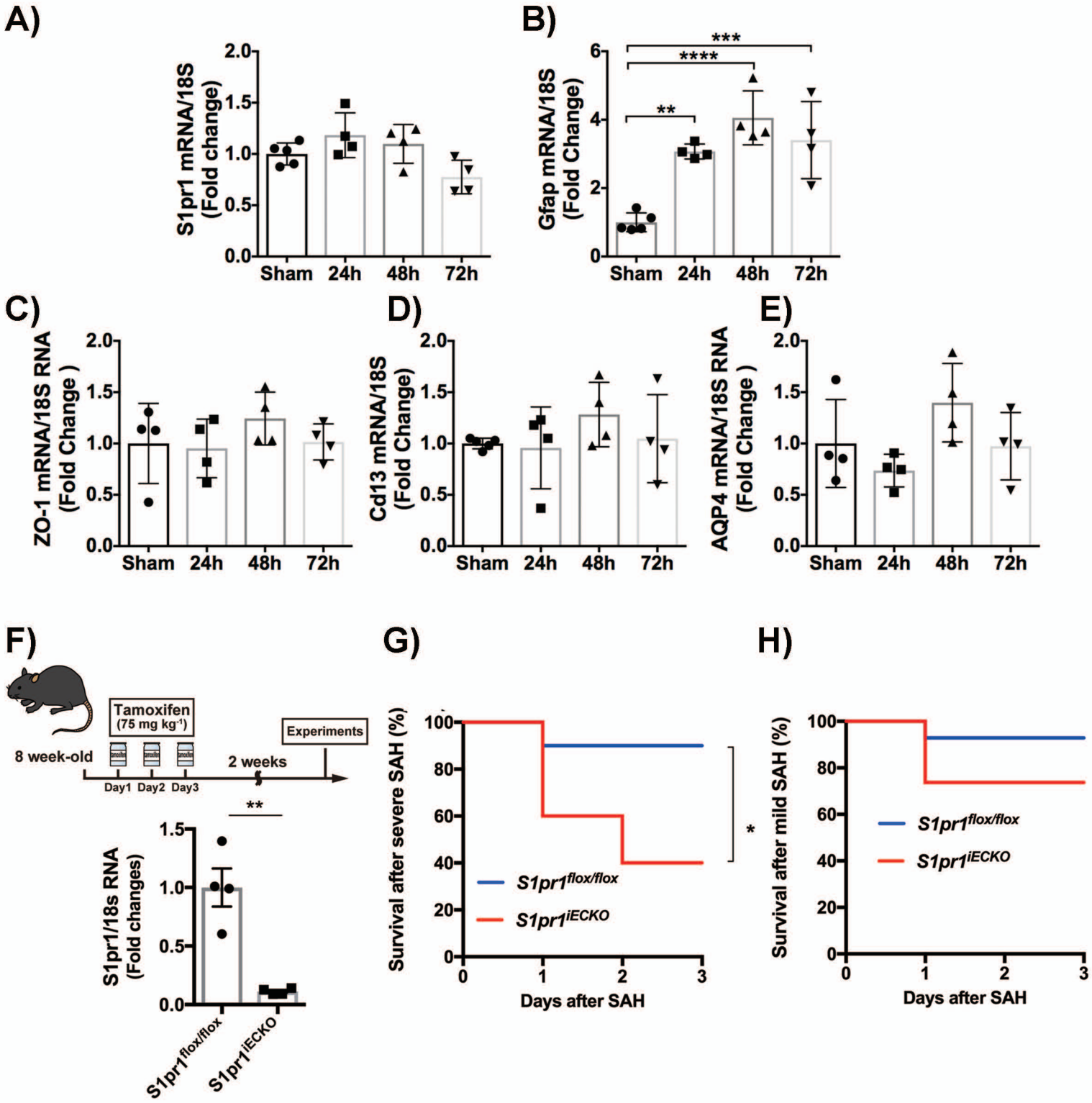
A)
S1pr1 mRNA/18S (Fold change)
2.0
1.5
1.0
0.5
0.0
Sham
24h
48h
72h
B)
Gfap mRNA/18S (Fold Change)
6
4
2
0
***
****
**
Sham
24h
48h
72h
C)
ZO-1 mRNA/18S RNA (Fold Change)
2.0
1.5
1.0
0.5
0.0
Sham
24h
48h
72h
D)
Cd13 mRNA/18S (Fold Change)
2.0
1.5
1.0
0.5
0.0
Sham
24h
48h
72h
E)
AQP4 mRNA/18S RNA (Fold Change)
2.0
1.5
1.0
0.5
0.0
Sham
24h
48h
72h
F)
Tamoxifen
(75 mg kg-1)
Experiments
8 week-old
2 weeks
Day1 Day2 Day3
**
S1pr1/18s RNA (Fold changes)
1.5
1.0
0.5
0.0
S1pr1flox/flox
S1pr1iECKO
G)
Survival after severe SAH (%)
100
80
60
40
20
0
0
1
2
3
Days after SAH
S1pr1flox/flox
S1pr1iECKO
*
H)
Survival after mild SAH (%)
100
80
60
40
20
0
0
1
2
3
Days after SAH
S1pr1flox/flox
S1pr1iECKO

Figure 4

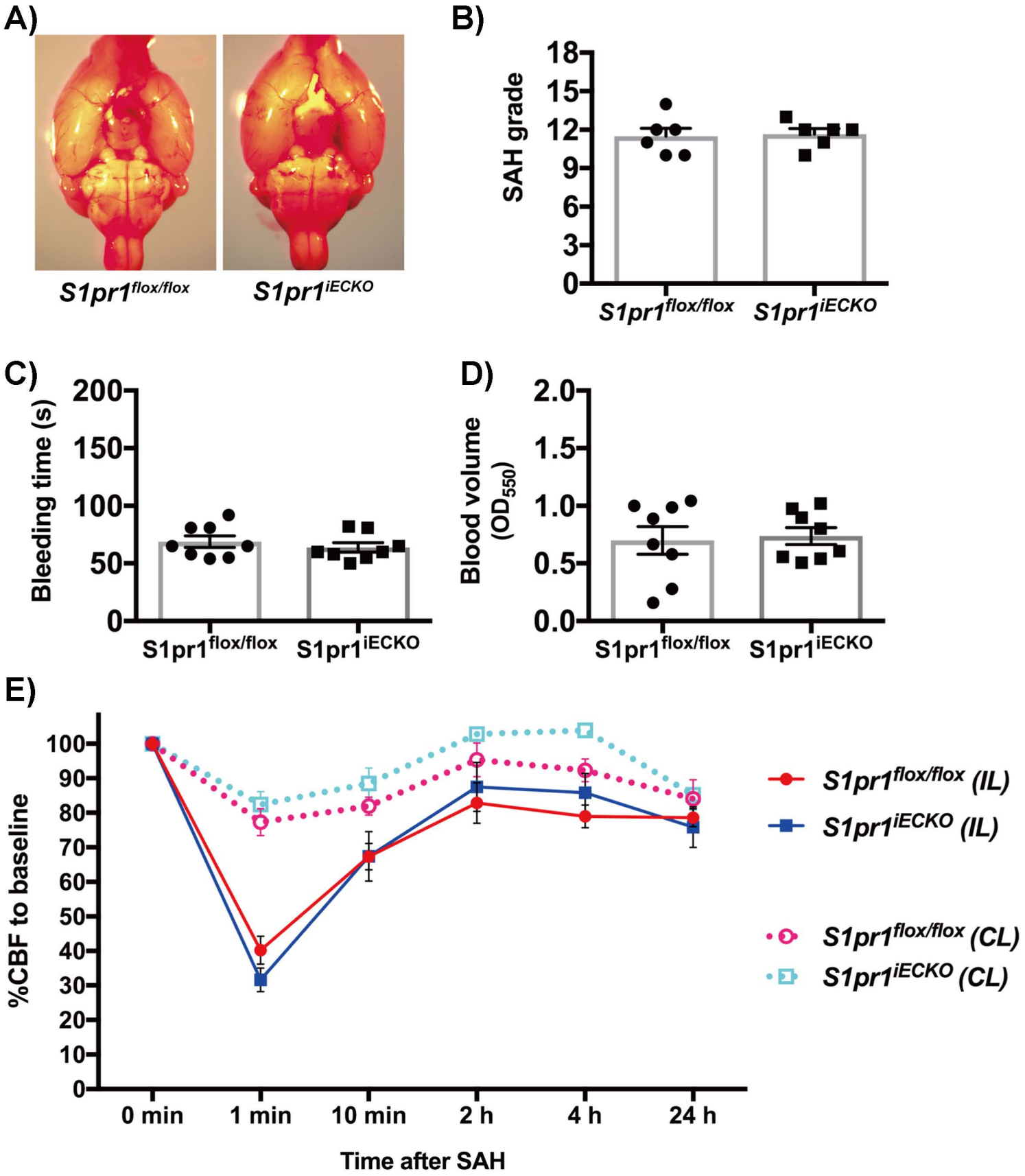
A)
S1pr1flox/flox
S1pr1iECKO
B)
SAH grade
18
15
12
9
6
3
0
S1pr1flox/flox
S1pr1iECKO
C)
Bleeding time (s)
200
150
100
50
0
S1pr1flox/flox
S1pr1iECKO
D)
Blood volume (OD550)
2.0
1.5
1.0
0.5
0.0
S1pr1flox/flox
S1pr1iECKO
E)
%CBF to baseline
100
90
80
70
60
50
40
30
20
10
0
0 min
1 min
10 min
2 h
4 h
24 h
Time after SAH
S1pr1flox/flox (IL)
S1pr1iECKO (IL)
S1pr1flox/flox (CL)
S1pr1iECKO (CL)

Figure 5

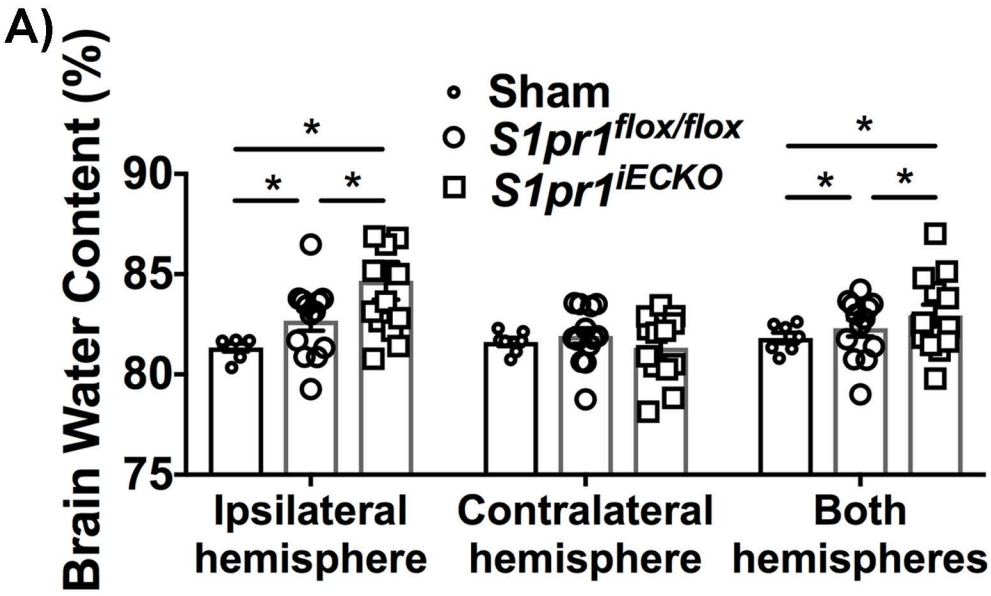
A)
Brain Water Content (%)
Sham
S1pr1flox/flox
S1pr1iECKO
90
85
80
75
*
*
*
*
*
Ipsilateral hemisphere
Contralateral hemisphere
Both hemispheres

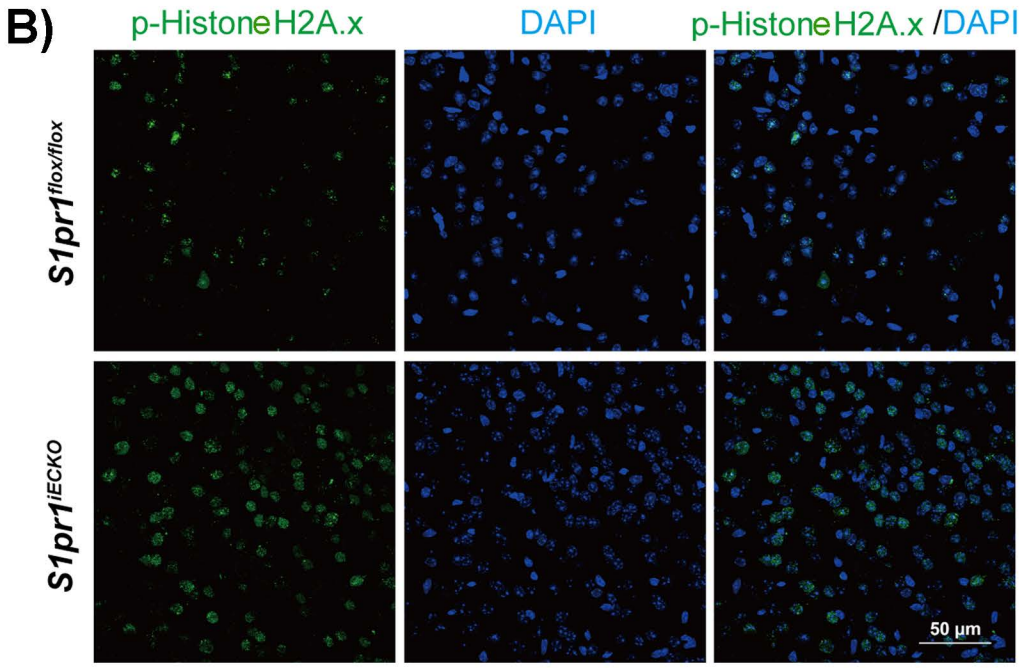
B)
p-HistoneH2A.x
DAPI
p-HistoneH2A.x /DAPI
S1pr1flox/flox
S1pr1iECKO
50 μm

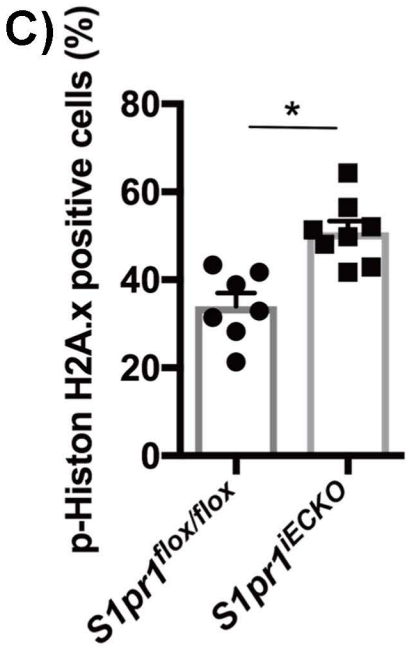
C)
p-Histon H2A.x positive cells (%)
80
60
40
20
0
*
S1pr1flox/flox
S1pr1iECKO

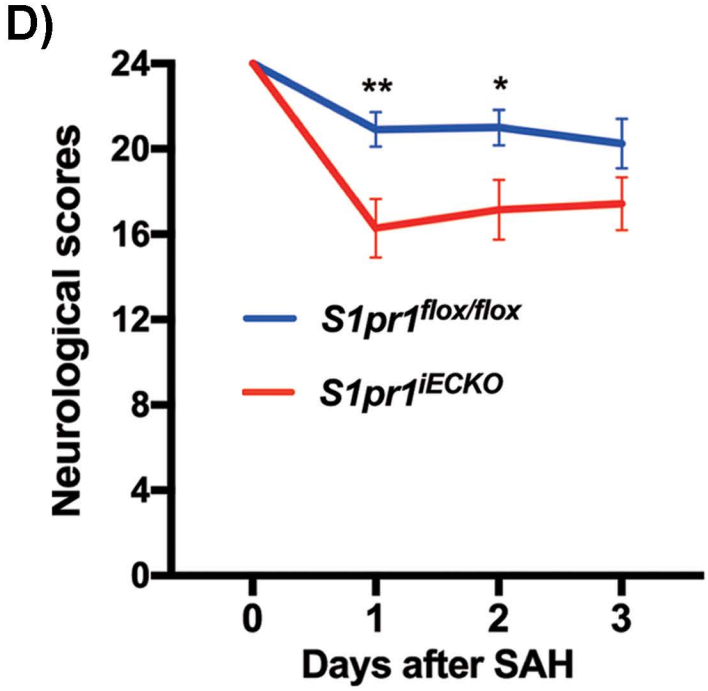
D)
Neurological scores
24
20
16
12
8
4
0
**
*
S1pr1flox/flox
S1pr1iECKO
0
1
2
3
Days after SAH

Figure 6

A

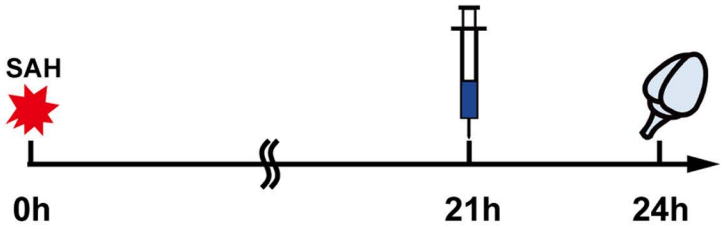
SAH
0h
21h
24h

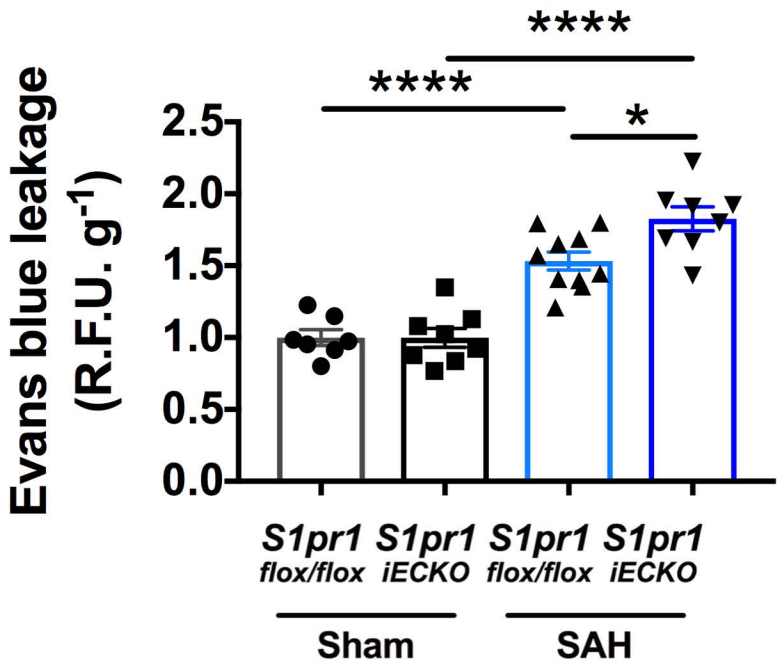
****
****
*
Evans blue leakage
(R.F.U. g-1)
2.5
2.0
1.5
1.0
0.5
0.0
S1pr1 flox/flox
S1pr1 iECKO
S1pr1 flox/flox
S1pr1 iECKO
Sham
SAH

B

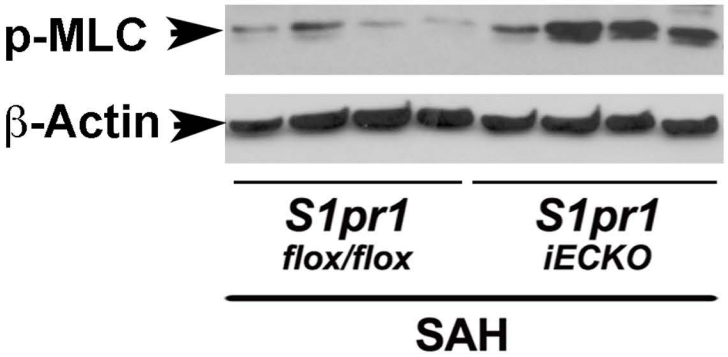
p-MLC
β-Actin
S1pr1 flox/flox
S1pr1 iECKO
SAH

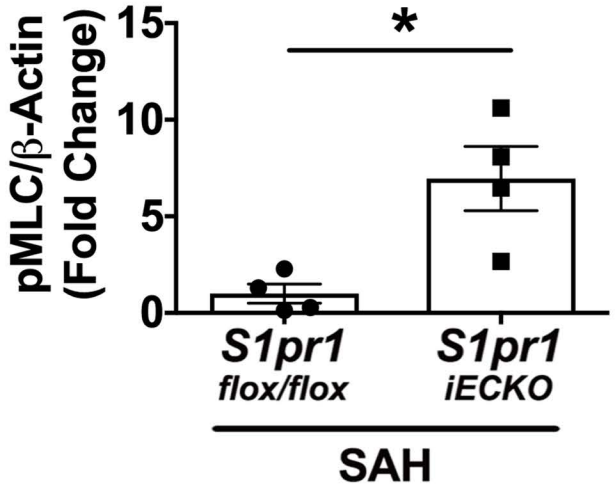
*
pMLC/β-Actin
(Fold Change)
15
10
5
0
S1pr1 flox/flox
S1pr1 iECKO
SAH

Figure 7